HHS Public Access

Author manuscript

Nat Immunol. Author manuscript; available in PMC 2018 August 26.

Published in final edited form as:

Nat Immunol. 2018 April ; 19(4): 407–419. doi:10.1038/s41590-018-0056-8.

Regulation of Age-associated B cells by IRF5 in systemic autoimmunity

Michela Manni[1], **Sanjay Gupta**[1], **Edd Ricker**[2], **Yurii Chinenov**[3,4], **Sung Ho Park**[3,4], **Man Shi**[1], **Tania Pannellini**[5], **Rolf Jessberger**[6], **Lionel Ivashkiv**[2,3,4,7], and **Alessandra B. Pernis**[1,2,4,7]

[1]Autoimmunity and Inflammation Program, Hospital for Special Surgery, NY, NY, USA

[2]Graduate Program in Immunology and Microbial Pathogenesis, Weill Cornell Graduate School of Medical Sciences, NY, NY, USA

[3]Arthritis and Tissue Degeneration Program, Hospital for Special Surgery, NY, NY, USA

[4]David Z. Rosensweig Genomics Research Center, Hospital for Special Surgery, NY, NY, USA

[5]Research Division and Precision Medicine Laboratory, Hospital for Special Surgery, NY, NY, USA

[6]Institute of Physiological Chemistry, Technische Universität, Dresden, Germany

[7]Department of Medicine, Weill Cornell Medical College, Cornell University, NY, NY, USA

Abstract

Age-associated B cells (ABCs) are a T-bet–dependent B cell subset, which accumulates prematurely in autoimmune settings. The pathways regulating ABCs in autoimmunity are largely unknown. SWAP-70 and DEF6 (also known as IBP or SLAT) are the only two members of the SWEF family, a unique family of Rho GTPase-regulatory proteins that controls both cytoskeletal dynamics and IRF4 activity. Notably, *DEF6* is a newly identified human SLE-risk variant. Here we show that the lupus syndrome that developed in SWEF-deficient mice is accompanied by the accumulation of ABCs, which produce autoantibodies upon stimulation. ABCs from SWEF-deficient mice exhibited a distinctive transcriptome and a unique chromatin landscape characterized by enrichment in motifs bound by transcription factors of the IRF family, AP-1/BATF, and T-bet. Enhanced ABC formation in SWEF-deficient mice was controlled by interleukin 21 (IL-21) and IRF5, whose variants are strongly associated with lupus. The lack of SWEF proteins led to dysregulated IRF5 activity in response to IL-21 stimulation. These studies thus uncover a new genetic pathway controlling ABCs in autoimmunity.

Correspondence should be addressed to A.B.P. (pernisa@hss.edu**).**

Author Contributions

M.M. designed and performed the experiments, interpreted the experiments and wrote the manuscript. S.G., E.R. and M.S. performed the experiments. Y.C. conducted the RNA-seq bioinformatics analysis. S.H.P conducted the ATAC-seq bioinformatics analysis. T.P. assisted with the histological analysis. R.J. generated the *Swap-70*$^{-/-}$ mice and helped write the manuscript. L.I. supervised the bioinformatics analysis and helped write the manuscript. A.B.P. designed and supervised the study, interpreted the experiments, and wrote the manuscript.

Competing Financial Interests

The authors declare no competing financial interests.

Aberrant humoral responses play a key role in the pathogenesis of systemic lupus erythematosus (SLE)[1]. While expansion of germinal center (GC) B cells and plasma cells (PC) has long been associated with SLE, additional B cell subsets may also contribute to disease. Studies in aging mice have identified a B cell subset, termed Age-associated B cells (ABCs), which exhibits a unique phenotype and preferentially expands in females with age[2–4]. In addition to classical B cell markers, ABCs also express the myeloid markers CD11c and CD11b[2–4]. ABC formation is promoted by TLR7/9 engagement, interferon-γ (IFN-γ), and interleukin 21 (IL-21)[3,5,6]. While ABCs exhibit somatic hypermutation[7], their relationship with GC B cells and PCs is not yet understood. ABCs increase prematurely in murine lupus and produce anti-chromatin antibodies[2,8]. ABC-like B cells (which include $IgD^{-}CD27^{-}$ and $CD21^{-/lo}$ B cells) have been detected in human autoimmune disorders including SLE[4,9,10]. ABCs express T-bet and depend on this transcription factor for their generation hence are also known as $CD11c^{+}$T-bet^{+} B cells[6,11] The molecular pathways that promote the expansion and pathogenicity of ABCs in autoimmunity are largely unknown.

Several interferon regulatory factors (IRFs) have been implicated in autoimmunity[12,13]. Amongst the IRFs, IRF4 plays a fundamental role in T and B cells including IL-21 production, class switching, and PC differentiation[12,13]. The multifaceted role of IRF4 has been ascribed to its capacity to cooperate with multiple transactivators like the AP-1 family members, BATF and Jun, and the Ets protein PU.1 (ref.[14]). Genetic studies have also demonstrated strong associations between variants of *IRF5* and human autoimmune disorders, particularly SLE[15,16]. Furthermore, *Irf5* deficiency ameliorates murine lupus in several models[17–20]. IRF5 is expressed in myeloid cells and regulates M1 macrophage polarization and the production of IFN-α and of proinflammatory cytokines[15,16,21]. Estrogen can modulate the abundance of IRF5 in B cells[22] where IRF5 regulates class switching to IgG2a/c and expression of the transcription factor Blimp1[19,23].

While searching for IRF4-interacting proteins, we isolated a protein termed DEF6 (also known as IBP or SLAT)[24–26]. DEF6 exhibits significant homology to only one other protein, SWAP-70[24–27]. SWAP-70 and DEF6 constitute the SWEF family, a unique family of Rho GTPase-regulatory proteins that controls both cytoskeletal dynamics and IRF4 activity[24–30]. Notably, the *DEF6* locus has been identified as a genetic risk factor for human SLE[31]. The SWEF proteins play an important immunoregulatory role and the concomitant lack of *Def6* and *Swap-70* in C57BL/6 mice (double knockouts, DKOs) leads to the spontaneous development of lupus, which, like human SLE, preferentially affects females[32]. Autoimmunity in DKOs is associated with dysregulation of T and B cells, increased IL-21 production, and enhanced formation of GC B cells and PCs[32].

Since ABCs accumulate in autoimmune mice we investigated this B cell subset in DKOs. DKOs exhibited an IL-21-dependent expansion of proliferating ABCs with proinflammatory capabilities. DKO ABCs produced autoantibodies and, compared to wild-type ABCs, displayed a distinctive transcriptome marked by increased immunoglobulin gene transcription and diminished expression of a subset of myeloid-related programs. DKO ABCs exhibited a unique chromatin landscape enriched in open chromatin regions containing IRF, AP-1/BATF, and T-bet binding motifs. In the absence of the SWEF proteins, IL-21 stimulation of B cells led to dysregulated IRF5 activity and the generation of ABCs.

Furthermore, ABC expansion and lupus development in DKO female mice was controlled by IRF5. Thus, IRF5 is a novel regulator of ABCs in autoimmune settings.

RESULTS

Spontaneous expansion of ABCs in DKO mice.

The spontaneous development of autoimmunity in DKO female mice led us to investigate whether ABCs accumulate prematurely in DKOs. Compared to wild-type mice, the frequencies and numbers of splenic B cells expressing CD11c and CD11b were markedly increased in DKO female mice irrespective of the gating strategy (Fig. 1a). Accumulation of these cells was not due to increases in plasmacytoid dendritic cells (Supplementary Fig. 1a). While wild-type ABCs are normally detected after 12 months of age[4], DKO ABCs started appearing by 10 weeks of age (Supplementary Fig. 1b) and comprised ≈10% of splenic B cells in older mice (Fig. 1a). Minimal ABC expansion was detected in DKO lymph nodes (Supplementary Fig. 1c). Mice lacking either *Def6* or *Swap-70* alone did not exhibit significant increases in ABCs (Fig. 1b). Thus, the premature expansion of $CD11c^+CD11b^+$ B cells observed *in vivo* in DKO mice requires the concomitant absence of both SWEF proteins.

We next examined the expression of several markers whose presence or absence defines ABCs[2–4]. The expression of T-bet was significantly higher in $CD11c^+CD11b^+$ than $CD11c^-CD11b^-$ DKO B cells (Fig. 1c) and corresponded to a marked expansion of $CD11c^+$T-bet^+ B cells in DKOs (Supplementary Fig. 1d). Moreover, $CD11c^+CD11b^+$ DKO B cells downregulated CD21 and CD23, displayed biphasic IgD expression, high amounts of IgM, CD86, and MHCII, and did not express CD43, CD93, or CD5 (Fig. 1c). While most $CD11c^+CD11b^+$ DKO B cells expressed IgM, a small number expressed IgG1 and IgG2c (Supplementary Fig. 1e). Thus, $CD11c^+CD11b^+$ DKO B cells express all the typical phenotypic features of previously described murine ABCs[2–4], including high T-bet expression, and will henceforth be termed ABCs.

To assess the ability of ABCs to produce autoantibodies, ABCs from DKOs were sorted (Supplementary Fig. 1f) and cultured *in vitro* with the TLR7 agonist, imiquimod. ABCs, but not follicular B cells (FoB) from DKOs, secreted anti-dsDNA IgG2c but not IgG1 upon stimulation (Fig. 1d and data not shown). Stimulated DKO ABCs also produced anti-nuclear ribonuclear protein (nRNP) and anti-cardiolipin IgG antibodies (Fig. 1d). ABCs could thus directly contribute to lupus in DKOs by producing autoantibodies.

IL-21 regulates the generation of DKO ABCs *in vitro* and *in vivo*.

Generation of murine ABCs can be promoted by IL-21 and TLRs[3,5,6]. We thus directly investigated the ability of these signals to drive ABC formation *in vitro* from B cells of young wild-type and DKO mice. Addition of IL-21, but not imiquimod, resulted in a significantly greater population of $CD11c^+$T-bet^+ ABCs in cultures of DKO than wild-type B cells (Fig. 2a). Similar results were obtained by using CD11c and CD11b as markers (Supplementary Fig. 2a). As reported[5], stimulation of wild-type and DKO B cells with either IL-4 or IFN-γ alone did not generate $CD11c^+$T-bet^+ B cells and addition of IL-4 inhibited

the IL-21-mediated formation of these cells in both wild-type and DKO cultures (Supplementary Fig. 2b). DKO B cells therefore exhibit an increased ability to generate ABCs *in vitro* upon IL-21 stimulation.

To further evaluate the importance of IL-21 in the expansion of DKO ABCs we examined DKO female mice lacking *Il21* (*Il21*$^{-/-}$ DKO). ABC accumulation was completely abrogated in these mice as compared to age-matched female DKOs (Fig. 2b). *Il21*$^{-/-}$ DKOs also failed to accumulate T_{FH} cells, GC B cells, and PCs and did not produce anti-dsDNA autoantibodies (Fig. 2d and Supplementary Fig. 2c-f). In addition to T_{FH} cells, IL-21 can also be produced by innate sources[33]. To determine whether direct T-B contacts were necessary for the expansion of DKO ABCs *in vivo,* we assessed their presence in DKOs lacking the SLAM-associated protein SAP (*Sap*$^{-/-}$ DKO), which mediates sustained T-B interactions[34]. The absence of *Sap* in DKOs strongly inhibited accumulation of ABCs, T_{FH} cells, GC B cells, PCs, and autoantibody production (Fig. 2c-d and Supplementary Fig. 2c-f). Thus, the aberrant expansion of DKO ABCs is dependent on IL-21 and cognate T-B cell interactions.

The SWEF proteins regulate the proliferation and proinflammatory capacity of ABCs.

To gain insights into the mechanisms by which the SWEF proteins regulate ABCs, we next sorted B cells based on the expression of CD11c and CD11b and employed RNA-seq to compare the transcriptomes of wild-type FoBs, DKO FoBs, and DKO ABCs. A total of 3049 genes were differentially expressed among the three different populations (logFC=1; FDR<0.01) (Fig. 3a). A set of genes were either upregulated (cluster 2) or downregulated (cluster 1) in DKO B cells irrespective of CD11c and CD11b expression suggesting that the lack of SWEF proteins altered the expression of these genes in B cells independently of their differentiation state (Fig. 3a). Based on gene set enrichment analysis (GSEA) (Fig. 3b, Supplementary Fig. 3a) the lack of the SWEF proteins affected the control of B cell proliferation, potentially, via E2F family of transcription factors and regulators of the G2/M checkpoint. Assessment of proliferation by Ki67 staining revealed that compared to wild-type B cells, CD11c^{-}T-bet^{-} DKO B cells contained a small population of highly proliferative cells (Fig. 3c). DKO ABCs proliferated even more robustly than CD11c^{-}T-bet^{-} DKO B cells (Fig. 3c). No differences in apoptosis were instead observed (Supplementary Fig. 3b). *In vitro* experiments demonstrated that DKO ABCs proliferated to a greater extent than wild-type ABCs upon stimulation with IL-21 (Supplementary Fig. 3c) while exhibiting similar survival (Supplementary Fig. 3d-e). Thus, the SWEF proteins regulate the proliferation of B cells and play an important role in restraining ABC proliferation in response to IL-21.

In addition to DKO-specific clusters 1 and 2, clusters 3 and 5 were uniquely regulated in DKO ABCs compared to FoBs from either wild-type or DKO mice (Fig. 3a and 3d). As expected, DKO ABCs exhibited higher expression of *Tbx21*, *Itgax,* and *Itgam* compared to FoBs (Fig. 3d). GSEA indicated that among the top enriched sets (FDR, q<0.05) in DKO ABCs relative to FoBs several gene sets were related to control of inflammation, chemotaxis, integrin binding, and cell adhesion (Fig. 3d-e, Supplementary Fig. 3f). Prominent among the upregulated genes were a number of chemokines (e.g. *Cxcl9, Cxcl10, Ccl5*), cytokine receptors (e.g. *Il1r2, Il12rb2, Il18r1*) and cytokines (Fig. 3d, Supplementary

Fig. 3f), some of which were further validated by qPCR in sorted cells (Fig. 3f). Thus, compared to FoBs, DKO ABCs are endowed with increased proinflammatory capabilities and unique migratory and adhesive attributes.

The chromatin landscape of DKO ABCs is enriched in IRF and AP-1/BATF motifs.

We next employed ATAC-seq[35] to interrogate the chromatin landscape of DKO ABCs. ATAC-seq signals from DKO ABCs were compared to DKO FoBs sorted from the same mice (Fig. 4a). We identified 3,666 ABC-specific peaks that were primarily found in intergenic and intronic regions and only rarely in promoters (Fig. 4b). Loci that were differentially accessible in ABCs as compared to FoBs included a number of proinflammatory cytokines like *Ifng* and *Il6* and other targets like the *Cxcl10* cluster of genes (Fig. 4c). ABC-specific peaks were positively associated with transcriptionally active genes in DKO ABCs as compared to DKO FoBs and pathway analysis showed that many of the differentially expressed ATAC-seq associated genes were involved in locomotion and cellular adhesion (Supplementary Fig. 4a-c).

To gain insights into the mechanisms underlying the distinctive chromatin profile of DKO ABCs, we determined the transcription factor binding motifs overrepresented in ABC-specific peaks (Fig. 4d). ABC-specific accessible loci displayed enrichment in AP-1/BATF, IRF, and T-bet binding motifs (Fig. 4d). The ABC-specific peaks exhibited substantial positional bias in the distribution of IRF and T-bet binding motifs, which coincided with the peak summit (Fig. 4e). In contrast, FoB-specific peaks exhibited enrichment in motifs for a distinct set of transcription factors including POU2F2 (Fig. 4d,e). Thus, DKO ABCs exhibit a unique chromatin landscape, which, in addition to T-bet motifs, is enriched in IRF and AP-1/BATF motifs and correlates with a distinctive transcriptional profile.

Distinctive transcriptional and epigenomic programs of autoimmune-prone DKO ABCs.

We next investigated whether the transcriptional profiles of autoimmune-prone DKO ABCs differed from those of ABCs that slowly accumulate in aging wild-type female mice. ABCs from wild-type and age-matched DKOs had similar expression of *Tbx21* (Supplementary Fig. 5a). A total of 711 genes were differentially expressed between the two populations (logFC=1, FDR<0.01), of which 111 genes were upregulated in DKO ABCs compared to wild-type ABCs and 600 genes were downregulated (Fig. 5a). DKO ABCs expressed several immunoglobulin gene transcripts more abundantly than wild-type ABCs, but downregulated a subset of myeloid-related transcripts (Fig. 5a-b and Supplementary Table 1). No changes in the expression of key regulators of PC differentiation like *Irf4*, *Irf8*, *Bcl6*, or *Prdm1* (Supplementary Fig. 5a) were detected in DKO ABCs suggesting that the differences were not due to the presence of contaminating plasmablasts. DKO ABCs, however, exhibited alterations in other transcription factors including upregulation of *Jun* and *Nfil3* and downregulation of *Maf*, *Mafb*, and *Pparg* while *Spi1* expression was similar to wild-type ABCs (Fig. 5c and Supplementary Fig. 5a). Differential expression of selected targets, including key regulators of apoptotic cell engulfment like *Mertk* and *Axl*, was further confirmed by qPCR (Fig. 5c). Thus, autoimmune-prone DKO ABCs are endowed with a higher immunoglobulin producing capacity than wild-type ABCs, but downregulate some of the myeloid-related features associated with this B cell subset.

To determine the differences in the chromatin landscape of wild-type and DKO ABCs that might accompany these distinct transcriptional profiles, ATAC-seq signals from sorted wild-type ABCs were compared to those of age-matched DKO ABCs. We identified 27,483 wild-type ABC-specific peaks and 1,583 DKO-ABC specific peaks (Fig. 5d). Most of the wild-type or DKO ABC-specific peaks were primarily found in intergenic and intronic regions and only rarely in promoters (Supplementary Fig. 5b). DKO ABC-specific accessible loci displayed enrichment in IRF, AP-1/BATF, and T-bet binding motifs (Fig. 5e). In contrast, wild-type ABC-specific peaks were associated with enrichment in PU.1, MAF, and C/EBP binding motifs (Fig. 5e). These results were consistent with the downregulation of *Maf* and *Mafb* observed in DKO ABCs and were reflected in differences in the accessibility of the *Maf* and *Mafb* loci detected by ATAC-seq (Supplementary. 5c). Gene ontology (GO) categories of genes associated with wild-type- or DKO-specific peaks indicated that wild-type ABC-specific peaks were positively associated with transcriptional programs regulating phagocytosis and other myeloid-related functions while DKO ABC-specific peaks were enriched in processes linked to B cell differentiation, activation, and Ig regulation (Fig. 5f). These findings support the idea that the differential chromatin accessibility between wild-type and DKOs ABCs is functionally important. Thus, compared to wild-type ABCs, the chromatin landscape of autoimmune-prone ABCs is characterized by dual abnormalities whereby enrichment in IRF and AP-1/BATF motifs is coupled with depletion of PU.1- and MAF-bound regulatory regions.

IRF5 regulates the IL-21-mediated formation of DKO ABCs.

The enrichment of IRF motifs in the chromatin landscape of DKO ABCs suggested that IRFs might contribute to the generation and/or function of ABCs. Since the SWEF proteins can regulate IRF4 activity[32,36,37], we first investigated whether DKO ABCs depend on IRF4. An analysis of *Cd11c*-Cre *Irf4*$^{fl/fl}$ DKO mice, previously generated to evaluate DCs[37], revealed that deleting *Irf4* in CD11c^{+}-expressing cells did not significantly affect ABC accumulation (Supplementary Fig. 6a) or other autoimmune parameters[37], suggesting that DKO ABCs may not require *Irf4*.

Given the homology amongst IRF DNA binding domains we next pursued the possibility that another IRF may regulate DKO ABCs. We focused on IRF5 given its ability to regulate the production of IgG2a/c and IL-6 and the strong association of *IRF5* variants with SLE[15,16]. To facilitate our studies, we generated DKOs lacking *Irf5* in B cells (*Cd21*-Cre *Irf5*$^{fl/-}$ DKO) and then assessed formation of ABCs *in vitro*. *Irf5* expression was similar in wild-type and DKO B cells and was absent in B cells from *Cd21*-Cre *Irf5*$^{fl/-}$ DKO mice (Supplementary Fig. 6b). Lack of *Irf5* markedly diminished the IL-21-driven ability of DKO B cells to generate ABCs (Fig. 6a,b) and produce IL-6, CXCL10, and IgG2c (Fig. 6c-e), but did not affect IgG1 production (Fig. 6e). Expression of *Jun*, a known IRF5 target[38], was also dysregulated in DKO B cells in an IL-21- and *Irf5*-dependent manner (Fig. 6f). Thus, the IL-21 driven abnormalities in ABC generation and function exhibited by DKO B cells are dependent on *Irf5*.

Since the ATAC-seq analysis had revealed an enrichment of IRF binding sites in ABC-specific peaks located at the *Il6* TSS, the *Cxcl10* cluster, the *Ighg2c* region, and *Jun*, we next

performed ChIP-assays to assess the binding of IRF5 to these regulatory regions. Compared to wild-type B cells, DKO B cells exhibited enhanced binding of IRF5 to these sites only upon stimulation with IL-21 (Fig. 7a and Supplementary Fig. 7a). IL-21-mediated STAT3 phosphorylation and the nuclear translocation of IRF5 were similar in WT and DKO B cells (Supplementary Fig. 7b,c). Minimal IRF5 binding was observed in *Cd21*-Cre *Irf5*$^{fl/-}$ DKO B cells supporting the specificity of the findings (Fig. 7a and Supplementary Fig. 7a). To evaluate whether ABC-specific peaks bound by IRF5 could also be targeted by T-bet, we performed ChIP-assays with a T-bet antibody (Fig. 7b and Supplementary Fig. 7a). DKO B cells exhibited increased binding of T-bet to the ABC-specific regions at the *Cxcl10* cluster, the *Ighg2c* peak, and *Jun* but not to the *Il6* TSS or a site in the *Zeb2* gene known not to bind T-bet[39]. Notably, *Irf5* deletion in DKO B cells resulted in decreased binding of T-bet to the *Cxcl10* cluster, the *Ighg2c* peak, and *Jun*. Further corroboration that IL-21 stimulation of DKO B cells leads to an aberrant ability of IRF5 and T-bet to target the *Cxcl10* cluster was obtained by performing oligonucleotide precipitation assays (ONPs). As observed with the ChIP assays, the presence of IRF5 was necessary for the ability of T-bet to bind to the *Cxcl10* cluster while no binding of T-bet to the *Il6* TSS could be detected (Fig. 7c and Supplementary Fig. 7d). Co-transfection of T-bet with IRF5 coupled with a mutational analysis confirmed that optimal recruitment of T-bet to the *Cxcl10* cluster requires DNA binding by IRF5 (Fig. 7d and Supplementary Fig. 7e). Taken together these findings support a model whereby, in the absence of the SWEF proteins, IL-21 stimulation leads to an increased ability of IRF5 to target ABC-specific peaks. Targeting of these regions by IRF5 subsequently enables recruitment of T-bet to a subset of these sites.

We next investigated the possibility that the SWEF proteins can interact with IRF5 and thus restrain its activity. Endogenous IRF5 in B cells was found to interact with both DEF6 and SWAP-70 (Fig. 7e). Association of IRF5 with either DEF6 or SWAP-70 mapped to the C-terminal portion of the SWEF proteins, which contains their IRF-interacting region, and required the IRF-association domain (IAD) of IRF5 (Supplementary Fig. 7f-h). No interaction of either DEF6 or SWAP-70 with T-bet was detected (Supplementary Fig. 7i). Co-transfections of IRF5 with DEF6 or SWAP-70 followed by ONP assays demonstrated that the full-length SWEF proteins, but not mutants unable to interact with IRF5, interfere with the ability of IRF5 to bind to the *Il6* TSS (Fig. 7f). In the course of these studies we also observed that DEF6 and SWAP-70 can heterodimerize (Supplementary Fig. 7j). These results suggest that interaction of IRF5 with the SWEF proteins can regulate IRF5 activity and thus indirectly alter the recruitment of T-bet to selected target genes.

Monoallelic deletion of *Irf5* abolishes accumulation of ABCs and lupus development in DKO mice.

We next evaluated the effect of *Irf5* deficiency on the *in vivo* expansion of DKO ABCs. Monoallelic deletion of *Irf5* significantly decreased ABC accumulation irrespective of the markers used (Fig. 8a,b and Supplementary Fig. 8a,b). Further deletion of *Irf5* using *Cd21*-Cre or *Cd11c*-Cre to target B cells or CD11c^{+} cells did not exert additional effects (Fig. 8a,b and Supplementary Fig. 8a-c). Loss of ABCs was accompanied by marked decreases in splenomegaly, T_{FH} cells, GC B cells, PCs, and autoantibodies (Fig. 8c-d and Supplementary Fig. 8d-f). Reduction in anti-dsDNA titers primarily reflected decreases in IgG2c rather than

IgG1 antibodies (Fig. 8d). Production of anti-ssDNA, anti-cardiolipin, and anti-nRNP autoantibodies was also markedly affected by the loss of *Irf5* (Fig. 8e). Diminished *Irf5* expression furthermore ameliorated several parameters of renal injury in DKO mice including expansion of mesangial matrix, presence of hyaline deposits, decrease in capillary loops, and deposition of immune complexes (Fig. 8f-g). Thus the aberrant expansion of DKO ABCs *in vivo* is dependent on *Irf5*. Furthermore, decreasing *Irf5* expression corrected several of the abnormalities observed in DKO female mice and markedly ameliorated the spontaneous development of lupus in these mice.

DISCUSSION

The molecular networks controlling ABCs in autoimmunity are largely unknown. Here we demonstrate that the SWEF proteins limit the generation of ABCs in response to IL-21. These cells exhibit a unique transcriptional profile and chromatin landscape enriched not only in T-bet binding sites but also in IRF and AP-1/BATF motifs. At a mechanistic level the SWEF proteins inhibit the IL-21-driven formation of ABCs by controlling the accessibility of IRF5 to key targets. These studies thus uncover a new pathway regulating ABCs in autoimmunity.

The lack of SWEF proteins results in abnormalities in several key processes including cell proliferation. This could promote both the premature accumulation of DKO ABCs and their dysregulated differentiation due to the close coupling between cell-division and the acquisition of B cell transcriptional and epigenetic programs[40]. Expansion of DKO ABCs could subsequently fuel autoimmunity via their dual capacity to secrete proinflammatory mediators and produce autoantibodies. Deletion of *Irf5* in DKOs, however, could have affected other subsets, like GC B cells and PCs, that produce autoantibodies and are dysregulated in DKOs[32]. Thus, it remains to be established whether DKO ABCs directly contribute to autoimmunity or whether their accumulation is secondary to the chronic inflammation of autoimmune conditions.

The distinctive features of autoimmune ABCs were highlighted by their unique chromatin landscape, which exhibited enrichment in IRF and AP-1/BATF binding sites in addition to the expected presence of T-bet motifs. These results were further supported by studies implicating IRF5 in the regulation of ABCs. Given the known interplay between AP-1 and IRFs[14], AP-1 proteins are also likely to be involved in the regulation of ABCs. An IRF5-AP-1 crosstalk could be further facilitated by a potential feed-forward loop set-up by the IRF5-mediated induction of *Jun*. Notably, the absence of the SWEF proteins resulted in increased binding of T-bet to several ABC-specific peaks, which occurred in an IRF5-dependent manner suggesting cooperativity between IRF5 and T-bet for at least some regulatory regions. This notion was reinforced by the requirement for the DNA binding domain of IRF5 in the optimal recruitment of T-bet to ABC-specific sites. It will need to be determined whether IRF5 can function as a focused pioneer factor for ABCs as shown for IRF1 in Tr1 cells[41].

The enrichment of IRF motifs in DKO ABC peaks was mechanistically linked to increased IRF5 activity due to lack of the inhibitory effects of the SWEF proteins. Both DEF6 and

SWAP-70 are found in the nucleus[32,42] suggesting that they inhibit the activity of nuclear IRF5, a finding supported by our biochemical studies. Given their ability to bind to the IAD of IRF5 they could also potentially interfere with its cross-talk with AP-1 proteins[14]. Previous studies showing that SWAP-70 can be recruited to some but not all IL-4-inducible promoters[42] furthermore suggest that the SWEF proteins could be recruited to distinct regulatory regions depending on the precise composition and/or modifications of SWEF-containing complexes. This may enable the SWEF inhibitory actions to specifically target either IRF4 or IRF5. The SWEF inhibitory effects may also depend on the relative abundance of IRF5 and IRF4, which could vary depending on the ABC differentiation stage. Indeed the IRF motifs within ABC-specific peaks could accommodate binding of other IRFs like IRF4, which could mark a more terminally differentiated ABC not captured by our present analysis. Given the role of IRF4 in GC B cells[43] we cannot furthermore exclude that IRF4 could be necessary at the earliest stages of ABC generation, which might not have been impacted by deleting *Irf4* in CD11c-expressing DKO cells[37]. Given the complex array of biological responses controlled by DEF6 and SWAP-70, the two SWEF proteins may also restrain ABCs *in vivo* by acting separately on additional IRF-independent pathways.

Compared to wild-type ABCs, autoimmune-prone ABCs also exhibited a marked loss of accessible chromatin regions containing PU.1, MAF, and C/EBP motifs. These changes were associated with downregulation of *Maf/Mafb* but not *Spi1*, a pattern reminiscent of that employed by IFN-γ to disassemble enhancers regulating M2-like macrophage programs [44]. This mechanism may be directly responsible for the decreased expression in DKO ABCs of *Mertk* and other myeloid-related targets involved in the engulfment of apoptotic cells, a pathway highly relevant to lupus pathogenesis. Given the known repressive role of PU.1 on antibody production and PC differentiation[45,46], selective depletion of PU.1-bound peaks could also lessen the PU.1-mediated inhibitory effects directly contributing to the increased levels of Ig transcription of DKO ABCs and endowing them with an enhanced ability to undergo PC differentiation upon exposure to environmental stimuli. Thus, dysregulated IRF5 activity coupled with the loss of PU.1-containing repressive complexes could represent a key mechanism employed by autoimmune-prone ABCs to bypass critical checkpoints governing the transition of B cells into antibody secreting cells.

While the role for IRF5 in TLR7 signaling is well-known[16], our studies now implicate IRF5 downstream of IL-21 thus positioning IRF5 as a common mediator of two key pathways for ABC generation in autoimmunity. The convergence of these pathways onto IRF5 is likely to contribute to the dramatic effects observed upon monoallelic deletion of *Irf5* on lupus development in ours and other models[18,20]. Such strong gene dosage effects may be particular relevant for human SLE where *IRF5* risk variants can affect *IRF5* expression[15,16].Associations between SLE and variants of *IL21*, *IL21R*, *DEF6*, and *IRF5* have all been identified in GWAS studies raising the intriguing possibility that improper regulation of this pathway plays a key role in SLE pathogenesis. Several polymorphisms in *DEF6*, which is located centromeric to the major histocompatibility complex[26], have been reported and expansion of ABC-like cells and aberrancies in *IL21/IL21R* or *IRF5* have also been observed in other autoimmune conditions like RA and IBD[4,47–50]. Dysregulation in the ability of the SWEF proteins to restrain IRF5 activity in response to IL-21 and properly control ABCs could thus contribute to multiple autoimmune diseases.

METHODS

Mice.

Female C57BL/6, *Cd21*-Cre and *Cd11c*-Cre mice were obtained from Jackson Laboratory. DEF6-deficient (*Def6*$^{tr/tr}$) mice were generated by Lexicon Pharmaceuticals, Inc. using a gene trapping strategy as previously described[32]. Swap-70-deficient mice (*Swap-70*$^{-/-}$) were generated as previously described[32]. *Def6*$^{tr/tr}$*Swap-70*$^{-/-}$ (DKO) mice were generated by crossing *Def6*$^{tr/tr}$ mice with *Swap-70*$^{-/-}$ mice that had been backcrossed onto C57BL/6 background for >10 generations[32]. *Sap*$^{-/-}$ mice were obtained from Taconic and crossed to DKO mice to obtain *Sap*$^{-/-}$ DKO mice. *Il21*$^{-/-}$ mice on mixed strain background were obtained from the Mutant Mouse Regional Resource Centers (Lexicon strain ID 011723-UCD), and then backcrossed into a C57BL/6 background for >10 generations and then crossed with DKO mice to obtain *IL21*$^{-/-}$ DKO mice. *Cd11c*-Cre *Irf4*$^{fl/fl}$ DKO mice were generated as previously described[37]. *Irf5*$^{fl/fl}$ mice, which do not carry the *Dock2* mutation, were originally obtained from P. Pitha-Rowe (Johns Hopkins University, MD)[23]. These mice were further crossed with DKO mice expressing either *Cd21*-Cre or *Cd11c*-Cre to produce *Irf5*$^{fl/fl}$ DKO, *Cd21*-Cre *Irf5*$^{fl/-}$ DKO, *Cd11c*-Cre *Irf5*$^{fl/-}$ DKO and *Irf5*$^{fl/-}$ DKO. All mice used in the experiments were kept under specific pathogen–free conditions. All the experiments were carried out following institutional guidelines and with protocols approved by the Institutional Animal Care and Use Committee of the Hospital for Special Surgery and WCMC/MSKCC.

Antibodies and flow cytometry.

The following monoclonal antibodies to mouse proteins were used for multi-parameter flow cytometry: CD11c (N418), CD11b (M1/70), CD19 (6D5), B220 (RA3–6B2), T-bet (4B10), CD4 (RM4–5), CD21/CD35 (7E9), CD23 (B3B4), CD86 (GL-1), MHCII (AF6–120.1), IgG1 (RMG1–1) and IgG2a (RMG2a-62) were obtained from BioLegend. Antibodies to CD43 (S7), CD138 (281–2), GL-7 and Fas (Jo2) were obtained from BD. Antibodies to Ki-67 (SolA15), IgD (11–26), IgM (II/41), CD93 (AA4.1), CD5 (53–7.3), PDCA-1 (eBio927), PD1 (J43) and Foxp3 (FJK-16s) were obtained from eBioscience. For staining of CXCR5 (2G8; BD), cells were incubated in dark at 25°C for 25 min. For intracellular staining, cells were fixed after surface staining at 4°C with the Foxp3 Staining Buffer Set (eBioscience) following the manufacturer instruction. For active caspase-3 staining, cells were stained using the CaspGLOW Active Caspase-3 Staining kit (BioVision) following the manufacturer instructions. For viability analysis, cells were stained with 0.5 μg of propidium iodide/samples prior to acquisition. Data were acquired on FACS Canto (Becton Dickinson) and analyzed with FlowJo (TreeStar) software.

Cell Sorting.

Single-cell suspensions from spleens were pre-enriched for B cells with B220 microbeads (Miltenyi Biotec) following the manufacturer instructions. B cells were stained with CD11c (N418), CD11b (M1/70), CD19 (6D5), B220 (RA3–6B2) and CD23 (B3B4) and were sorted on FACS Aria (Becton Dickinson).

B cell differentiation.

Single-cell suspensions from pooled spleens were enriched for B cells with biotinylated anti-CD23 (BD Bioscience) and streptavidin microbeads (Miltenyi Biotec) following the manufacturer instructions. $CD23^+$ B cells were cultured in RPMI 1640 medium (Corning) supplemented with 10% FBS (Atlanta Biologicals), 100 U/ml Penicillin (Corning), 100 mg/ml Streptomycin (Corning), 1X Non-Essential Amino Acids (Corning), 2 mM L-Glutamine (Corning), 25 mM HEPES (pH 7.2–7.6) and 50 μM β-Mercaptoethanol, and stimulated with 5 μg/ml $F(ab')_2$ anti-mouse IgM (αIgM; Jackson ImmunoResearch Laboratories), 5 μg/ml Ultra-LEAF purified anti-mouse CD40 (Biolegend), in presence or absence of 50 ng/ml IL-21 (Peprotech), 1 μg/ml imiquimod (Invivogen), 10 ng/ml IL-4 (Peprotech) or 20 ng/ml IFN-γ (Peprotech). For proliferation assays, $CD23^+$ B cells were labelled with 2.5 μM CFSE or Cell trace violet (Invitrogen) for 1 min at 25°C prior stimulation.

qPCR.

Total RNA was isolated from cells using RNeasy Plus Mini kit (Qiagen). cDNAs were prepared using the iScript cDNA synthesis kit (Bio-Rad). Real-Time PCR was performed using the iTaq Universal SYBR Green Supermix (Biorad). Gene expression was calculated using the ΔΔCt method and normalized to Cyclophilin a. *Lifr* and *Jun* primers were obtained from Qiagen. The following custom primers were used: *Ccl5 forward* 5′-GCCCACGTCAAGGAGTATTTCTA-3′, *Ccl5 reverse* 5′-ACACACTTGGCGGTTCCTTC-3′; *Il6 forward* 5′-GAGGATACCACTCCCAACAGAC-3′, *Il6 reverse* 5′-AAGTGCATCATCGTTGTTCATA-3′; *Cxcl10 forward* 5′-CCAAGTGCTGCCGTCATTTTC-3′, *Cxcl10 reverse* 5′-GGCTCGCAGGGATGATTTCAA-3′; *Ifng forw*ard 5′-GGATATCTGGAGGAACTGGC-3′, *Ifng reverse* 5′-GCGCCAAGCATTCAATGAGCTC-3′; *Spi1 forward* 5′-TGCAGCTCTGTGAAGTGGTT-3′, *Spi1 reverse 5′-AGCGATGGAGAAAGCCATAG-3′*, *Zbtb32 forward* 5′-TCCAGATACGGTGCTCCCTTCT-3′, *Zbtb32 reverse* 5′-CCAGAGAGCTTTGGAGTGGTTC-3′, *Nfil3 forward* 5′-AATTCATTCCGGACGAGAAG-3′, *Nfil3 reverse* 5′-CGATCAGCTTGTTCTCCAAA-3′, *Maf forward* 5′-AGCAGTTGGTGACCATGTCG-3′, *Maf reverse* 5′-TGGAGATCTCCTGCTTGAGG-3′, *Axl* forward 5′-CGAGAGGTGACCTTGGAAC-3′, *Axl reverse* 5′-AGATGGTGGAGTGGCTGTC-3′, *Mertk forward* 5′-GGCTTTTGGCGTGACCATG-3′*, Mertk reverse* 5′-AGTTCATCCAAGCAGTCCTC-3′, Cyclophilin A *Ppia forward* 5′-TTGCCATTCCTGGACCCAAA-3′, *Ppia reverse* 5′-ATGGCACTGGCGGCAGGTCC-3′.

DNA Constructs.

Expression plasmids for untagged and HA-tagged human DEF6 and its various deletion mutants were generated as described previously[32]. The full-length wild-type human SWAP-70 expression plasmid (pIRES2-EGFP-HA-SWAP70) was constructed by cloning the entire coding region of the human Swap-70 cDNA, fused in frame with a hemagglutinin

(HA) epitope coding sequence at its 5' end, into the pIRES2-EGFP bicistronic expression vector (Clonetech). Various deletion mutants of human SWAP-70 were generated by PCR using appropriate primers. The full-length wild-type human IRF5 expression construct in pcDNA3 was a kind gift of I. Rogatsky. Full length human IRF5 (variant 5) and T-bet expression constructs were purchased from Genscript. Expression plasmids for Flag-tagged IRF5 (variant 5) and its various deletion mutants were constructed in p3XFLAG-CMV-10 expression vector (Sigma) using IRF5 construct (Genscript) as a PCR template. Expression plasmid for untagged T-bet was generated in pIRES2-EGFP bicistronic expression vector (Clonetech) using T-bet expression construct (Genscript) as a PCR template.

Immunoblotting and Immunoprecipitation.

Nuclear and cytoplasmic extracts were prepared with NE-PER Nuclear and Cytoplasmic Extraction Reagents (Pierce), as previously described[32]. For expression analysis cell extracts were analyzed by immunoblotting with the following antibodies: anti-STAT3 (BD Bioscience), anti-pSTAT3 (Y705) (Cell Signaling), anti-IRF5 (Cell Signaling) or anti-HDAC1 (Cell Signaling). For protein-protein interaction studies, cell extracts were immunoprecipitated with an anti-IRF5 (Cell Signaling), or anti-HA (3F10; Roche Applied Science). The immunoprecipitates were resolved by 8% SDS-PAGE, transferred to a nitrocellulose membrane, and then immunoblotted with either an anti–SWAP-70 (Santa Cruz Biotechnology, Inc.), anti-DEF6 antiserum[26] or anti-HA (Roche Applied Science).

ChIP assays.

$CD23^+$ B cells were purified and stimulated in vitro for 48 h. After harvesting, the cells were cross-linked with formaldehyde, and chromatin extracts were prepared using the truChIP Chromatin Shearing Reagent Kit (Covaris) according to manufacturer instructions. The DNA–protein complexes were immunoprecipitated with an anti-IRF5 (Abcam, ab21689) or anti-T-bet (Santa Cruz; sc-21749X) specific antibody or a control antibody. After cross-linking was reversed and proteins were digested, the DNA was purified from the immunoprecipitates as well as from input extracts, and then analyzed by quantitative PCR using primers within the ABC-specific ATAC-seq peaks at the murine *Il6* TSS (Forward: 5′AGCTTCTCTTTCTCCTTATAAAACATTG-3′ and Reverse 5′-GCATCGAAAGAATCACAACTAGG-3′), the *Cxcl10* Cluster (Forward: 5′-AGTAGTCCCCACTGTCTGACT-3′ and Reverse: 5′-GTGAGTCCCTTTAGCACCAGA-3′), *Zeb2* Exon8 (Forward: 5′-AGCAGTCCCTTTATGAACGG-3′ and Reverse: 5′-GCTTCCATCCCTACACCTAAG-3′), *Jun* (Forward 5′-AGAACAGCTTTTGAGCACCG-3′ and Reverse 5′-TGGCTTCAAAGTGACTAACAGCA-3′) and *Ighg2c* (Forward 5′-TGTAATGCCTGGTTGCCTCC-3′ and Reverse 5′-GTTCGGGACCCACAGTACATT-3′).

ONP Assays.

ONP assays were conducted as previously described [51]. Briefly, nuclear extracts were precleared with streptavidin-agarose beads and then incubated with biotinylated double-stranded oligonucleotide containing potential IRF binding site within the ATAC-seq peak at the *Cxcl10* Cluster (5′-CATAGAAAATGTTTTCAAAACCCGCATTCCGCTTATGCTGTCTGGTATCTGAAATA

GATCTGTCAGGGGGTCACATTTTATAAGCACCACTTCGTGTTTG-3′) or *Il6* TSS (trimerized 5′- TGCTGAGTCACTTTTAAAGAAAAAAAGAAGAGT-3′). Proteins bound to the biotin-labeled DNA were collected by streptavidin-agarose beads, separated by 8% SDS-PAGE, and analyzed by immunoblotting using anti-mouse IRF5 (Cell signaling), anti-human IRF5 (Santa Cruz SC-390364) or an anti-T-bet (Santa Cruz; sc-21749) antibodies.

Cytokines and ELISA.

IL-6 and CXCL10 in culture supernatants were measured using the mouse ELISA Max Standard Set (BioLegend) and the mouse Quantikine ELISA kit (R&D Systems) respectively.

Autoantibody ELISA and ANA.

For anti-dsDNA ELISA, plates were coated with 100 μg/ml salmon sperm DNA (Invitrogen AM9680) at 37°C overnight and blocked in 2% BSA in PBS, at room temperature for 2 h. For anti-cardiolipin ELISA Immulon 2HB plates (Thermo Fisher) were coated with 75 μg/ml of cardiolipin dissolved in 100% ethanol at 25°C overnight. Sera were diluted 1:200 and incubated on coated plates at 25°C for 2 h. Plates were then incubated with horseradish peroxidase-labeled goat anti-mouse IgG, IgG1 or IgG2c Fc antibody for 1 h (eBioscience). Anti-ssDNA and anti-nRNP IgG ELISAs were obtained from Alpha Diagnostic International. OD_{450} was measured on a microplate reader. ANAs were detected on Hep-2 slides (MBL international) at a 1:200 dilution using Alexa Flour 488-conjugated anti-mouse IgG (Jackson ImmunoResearch Laboratories). Fluorescent intensity was semi-quantitated as previously described[52].

Histology and Immunofluorescence staining.

Tissue specimens were fixed in 10% neutral buffered formalin and embedded in paraffin. Tissue sections were stained with periodic acid schiff (PAS) and analyzed by light microscopy. The nephritis scoring system was adapted from the International Society of Nephrology/Renal Pathology Society (ISN/RPS) classification of human lupus nephritis. At least 40 glomeruli per mouse were evaluated. The final score accounted for morphological pattern (mesangial, capillary, membranous) and for the percentage of involved glomeruli. Immunofluorescence analysis on frozen kidney sections was performed by staining with FITC-labeled goat anti–mouse IgG (Jackson ImmunoResearch Laboratories) and specimens were analyzed with a LSM 510 laser scanning confocal microscope (Carl Zeiss, Inc.). Images were captured by Q capture software. Five representative glomeruli per mouse were chosen and mean fluorescent intensity (MFI) was calculated using ImageJ software.

RNA-Seq analysis.

Total RNA was isolated using RNeasy Plus Mini kit (Qiagen). SMART-Seq v3 Ultra Low Input RNA Kit (Clontech) followed by Nextera library preparation were used to prepare Illumina-compatible sequencing libraries. Quality of all RNA and library preparations were evaluated with BioAnalyser 2100 (Agilent). Sequencing libraries were pair-end sequenced by the Weill Cornell Epigenomics Core using HiSeq2500 at the depth of ~30–50 million fragments per sample. Sequencing performance was evaluated using FASTQC. 50-bp paired

reads were mapped to mouse genome (mm10, build 38.75, 41,128 genes and 87,108 transcripts) with CLC Bio Genomic Workbench 7.5 software (Qiagen). Duplicated reads with more than 5 copies were discarded. Read count tables were created using unique exon read counts and the differential expression was analyzed using EDGER (Bioconductor). Genes with the expression levels less than 1 count per million (cpm) in at least three conditions were considered non-expressing and removed from further analysis. A negative binomial generalized log-linear model was fit to read counts for each gene. A likelihood ratio tests with the null hypothesis that the pairwise contrasts of the coefficients are equal to zero was used to evaluate the significance of differences in expression between analyzed groups. Benjamini-Hochberg false discovery rate (FDR) procedure was used to correct for multiple testing. Genes with a FDR-corrected *P*-value > 0.01 and less than 2-fold change were filtered out. Genes that passed the filtering were considered to be differentially expressed.

Gene Set Enrichment Analysis (GSEA, http://www.broad.mit.edu/gsea/index.html) was performed using the difference of log-transformed count per million (cpm) for contrasted conditions as a ranking metric. Molecular Signatures DataBase v 5.2 (Broad Institute) was used as source of gene sets with defined functional relevance. Gene sets ranging between 15 and 1000 genes were included into analysis. Nominal *P*-values were FDR corrected and gene sets with FDR<0.05 were used to create GSEA enrichment plot. To define the groups of potentially co-regulated genes we performed unsupervised hierarchical clustering analysis of log-transformed expression values (cpm) in R. The distances between genes were calculated as (1 - Pearson correlation). The Euclidean distance was used to determine the distances between samples. Ward.D2 methods was used to performs clustering. The expression values were *z*-transformed and visualized using heatmaps.

ATAC-seq, peak calling and annotation.

The nuclei of sorted WT and DKO ABC or DKO Follicular B cells were prepared by incubation of cells with nuclear preparation buffer (0.30 M sucrose, 10 mM Tris, pH 7.5, 60 mM KCl, 15 mM NaCl, 5 mM $MgCl_2$, 0.1 mM EGTA, 0.1% NP40, 0.15 mM spermine, 0.5 mM spermidine and 2 mM 6AA) [53]. Libraries were prepared as described previously[35]. Paired-end 50bp sequences were generated from samples on an Illumina HiSeq2500. We used the *makeTagDirectory* followed by *findPeaks* command from HOMER version 4.7.2 (http://homer. salk.edu/homer/) to identify peaks of ATAC-seq. A false discovery rate (FDR) threshold of 0.001 was used for all data sets. The following HOMER command was used: cmd = *findPeaks* <sample tag directory> -style factor or histone -o <output file> -i <input tag directory>. The total number of mapped reads in each sample was normalized to ten million mapped reads. Peak-associated genes were defined based on the closest genes to these genomic regions using RefSeq coordinates of genes. We used the *annotatePeaks* command from HOMER to calculate ATAC-seq tag densities from different experiments and to create heatmaps of tag densities. Sequencing data were visualized by preparing custom tracks for the UCSC Genome browser.

Motif enrichment analysis.

De novo transcription factor motif analysis was performed with motif finder program *findMotifsGenome* from HOMER package, on given ATAC-seq peaks. Peak sequences were compared to random genomic fragments of the same size and normalized G+C content to identify motifs enriched in the targeted sequences.

Statistics.

P-values were calculated with unpaired two-tailed Student's t-test for two-group comparisons and by one-way ANOVA followed by Bonferroni's multiple comparisonss test for multi-group comparisons. For statistical analysis of ANA intensity score the non-parametric Mann-Whitney test was used. *P*-values of <0.05 were considered significant. Ns: not significant, *: $P < 0.05$, **: $P < 0.01$ ***: $P < 0.001$***: $P < 0.0001$. Statistical analysis was performed with Graphpad Prism 7.

Life science reporting summary.

Further information on experimental design and reagents is available in the Life Science Reporting Summary.

Data Availability.

The data that support the findings of this study are available from the corresponding author upon request. The RNA-seq and ATAC-seq sequencing data have been deposited at accession number GSE99480.

Supplementary Material

Refer to Web version on PubMed Central for supplementary material.

Acknowledgments

We thank I. Rogatsky for the full-length wild-type human IRF5 expression construct in pcDNA3P and the late P. Pitha-Rowe (Johns Hopkins University, MD) for the $Irf5^{fl/fl}$ mice. The research was supported by a gift in honor of Anne O'Neil (M.M.), an NIH F31 the Ruth L. Kirschstein National Service Award (E.R.), the US National Institutes of Health (AR064883 and AR070146 to A.B.P; AI044938 to L.I.), the Peter Jay Sharp Foundation, the Tow Foundation which provided support for the David Z. Rosensweig Genomics Research Center, Giammaria Giuliani and the Ambrose Monell Foundation. Technical support was provided by the Epigenomics Core and the Flow Cytometry Core Facility of Weill Cornell Medical College (Office of the Director of the National Institutes of Health under Award Number S10OD019986 to Hospital for Special Surgery).

REFERENCES

1. Liu Z & Davidson A Taming lupus-a new understanding of pathogenesis is leading to clinical advances. Nat Med 18, 871–882 (2012). [PubMed: 22674006]
2. Rubtsov AV et al. Toll-like receptor 7 (TLR7)-driven accumulation of a novel CD11c(+) B-cell population is important for the development of autoimmunity. Blood 118, 1305–1315 (2011). [PubMed: 21543762]
3. Hao Y , O'Neill P , Naradikian MS , Scholz JL & Cancro MP A B-cell subset uniquely responsive to innate stimuli accumulates in aged mice. Blood 118, 1294–1304 (2011). [PubMed: 21562046]
4. Naradikian MS , Hao Y & Cancro MP Age-associated B cells: key mediators of both protective and autoreactive humoral responses. Immunol Rev 269, 118–129 (2016). [PubMed: 26683149]

5. Naradikian MS et al. Cutting Edge: IL-4, IL-21, and IFN-gamma Interact To Govern T-bet and CD11c Expression in TLR-Activated B Cells. J Immunol 197, 1023–1028 (2016). [PubMed: 27430719]
6. Rubtsova K , Rubtsov AV , van Dyk LF , Kappler JW & Marrack P T-box transcription factor T-bet, a key player in a unique type of B-cell activation essential for effective viral clearance. Proc Natl Acad Sci U S A 110, E3216–3224 (2013). [PubMed: 23922396]
7. Russell Knode LM et al. Age-Associated B Cells Express a Diverse Repertoire of VH and Vkappa Genes with Somatic Hypermutation. J Immunol 198, 1921–1927 (2017). [PubMed: 28093524]
8. Rubtsov AV , Rubtsova K , Kappler JW & Marrack P TLR7 drives accumulation of ABCs and autoantibody production in autoimmune-prone mice. Immunol Res 55, 210–216 (2013). [PubMed: 22945807]
9. Wei C et al. A new population of cells lacking expression of CD27 represents a notable component of the B cell memory compartment in systemic lupus erythematosus. J Immunol 178, 6624–6633 (2007). [PubMed: 17475894]
10. Sanz I , Wei C , Lee FE & Anolik J Phenotypic and functional heterogeneity of human memory B cells. Semin Immunol 20, 67–82 (2008). [PubMed: 18258454]
11. Rubtsova K et al. B cells expressing the transcription factor T-bet drive lupus-like autoimmunity. J Clin Invest 127, 1392–1404 (2017). [PubMed: 28240602]
12. Rogatsky I , Chandrasekaran U , Manni M , Yi W & Pernis AB Epigenetics and the IRFs: a complex interplay in the control of immunity and autoimmunity. Autoimmunity 47, 242–255 (2014). [PubMed: 24215615]
13. Matta B , Song S , Li D & Barnes BJ Interferon regulatory factor signaling in autoimmune disease. Cytokine 98, 15–26 (2017). [PubMed: 28283223]
14. Murphy TL , Tussiwand R & Murphy KM Specificity through cooperation: BATF-IRF interactions control immune-regulatory networks. Nat Rev Immunol 13, 499–509 (2013). [PubMed: 23787991]
15. Lazzari E & Jefferies CA IRF5-mediated signaling and implications for SLE. Clin Immunol 153, 343–352 (2014). [PubMed: 24928322]
16. Cham CM , Ko K & Niewold TB Interferon regulatory factor 5 in the pathogenesis of systemic lupus erythematosus. Clin Dev Immunol 2012, 780436 (2012). [PubMed: 23251221]
17. Yasuda K et al. Interferon regulatory factor-5 deficiency ameliorates disease severity in the MRL/lpr mouse model of lupus in the absence of a mutation in DOCK2. PLoS One 9, e103478 (2014). [PubMed: 25076492]
18. Ban T et al. Lyn Kinase Suppresses the Transcriptional Activity of IRF5 in the TLR-MyD88 Pathway to Restrain the Development of Autoimmunity. Immunity 45, 319–332 (2016). [PubMed: 27521268]
19. Savitsky DA , Yanai H , Tamura T , Taniguchi T & Honda K Contribution of IRF5 in B cells to the development of murine SLE-like disease through its transcriptional control of the IgG2a locus. Proc Natl Acad Sci U S A 107, 10154–10159 (2010). [PubMed: 20479222]
20. Watkins AA et al. IRF5 deficiency ameliorates lupus but promotes atherosclerosis and metabolic dysfunction in a mouse model of lupus-associated atherosclerosis. J Immunol 194, 1467–1479 (2015). [PubMed: 25595782]
21. Ikushima H , Negishi H & Taniguchi T The IRF family transcription factors at the interface of innate and adaptive immune responses. Cold Spring Harb Symp Quant Biol 78, 105–116 (2013). [PubMed: 24092468]
22. Shen H et al. Gender-dependent expression of murine Irf5 gene: implications for sex bias in autoimmunity. J Mol Cell Biol 2, 284–290 (2010). [PubMed: 20802013]
23. Fang CM et al. Unique contribution of IRF-5-Ikaros axis to the B-cell IgG2a response. Genes Immun 13, 421–430 (2012). [PubMed: 22535200]
24. Hotfilder M , Baxendale S , Cross MA & Sablitzky F Def-2, −3, −6 and −8, novel mouse genes differentially expressed in the haemopoietic system. Br J Haematol 106, 335–344 (1999). [PubMed: 10460589]
25. Tanaka Y et al. SWAP-70-like adapter of T cells, an adapter protein that regulates early TCR-initiated signaling in Th2 lineage cells. Immunity 18, 403–414 (2003). [PubMed: 12648457]

26. Gupta S et al. Molecular cloning of IBP, a SWAP-70 homologous GEF, which is highly expressed in the immune system. Hum Immunol 64, 389–401 (2003). [PubMed: 12651066]
27. Borggrefe T , Wabl M , Akhmedov AT & Jessberger R A B-cell-specific DNA recombination complex. J Biol Chem 273, 17025–17035 (1998). [PubMed: 9642267]
28. Becart S & Altman A SWAP-70-like adapter of T cells: a novel Lck-regulated guanine nucleotide exchange factor coordinating actin cytoskeleton reorganization and Ca2+ signaling in T cells. Immunol Rev 232, 319–333 (2009). [PubMed: 19909373]
29. Biswas PS , Bhagat G & Pernis AB IRF4 and its regulators: evolving insights into the pathogenesis of inflammatory arthritis? Immunol Rev 233, 79–96 (2010). [PubMed: 20192994]
30. Ripich T et al. SWEF Proteins Distinctly Control Maintenance and Differentiation of Hematopoietic Stem Cells. PLoS One 11, e0161060 (2016). [PubMed: 27561029]
31. Sun C et al. High-density genotyping of immune-related loci identifies new SLE risk variants in individuals with Asian ancestry. Nature genetics 48, 323–330 (2016). [PubMed: 26808113]
32. Biswas PS et al. Dual regulation of IRF4 function in T and B cells is required for the coordination of T-B cell interactions and the prevention of autoimmunity. J Exp Med 209, 581–596 (2012). [PubMed: 22370718]
33. Vinuesa CG & Chang PP Innate B cell helpers reveal novel types of antibody responses. Nat Immunol 14, 119–126 (2013). [PubMed: 23334833]
34. Cannons JL , Tangye SG & Schwartzberg PL SLAM family receptors and SAP adaptors in immunity. Annu Rev Immunol 29, 665–705 (2011). [PubMed: 21219180]
35. Buenrostro JD , Wu B , Chang HY & Greenleaf WJ ATAC-seq: A Method for Assaying Chromatin Accessibility Genome-Wide. Curr Protoc Mol Biol 109, 21 29 21–29 (2015).
36. Chen Q et al. IRF-4-binding protein inhibits interleukin-17 and interleukin-21 production by controlling the activity of IRF-4 transcription factor. Immunity 29, 899–911 (2008). [PubMed: 19062315]
37. Manni M et al. IRF4-Dependent and IRF4-Independent Pathways Contribute to DC Dysfunction in Lupus. PloS one 10, e0141927 (2015). [PubMed: 26544714]
38. Kreher S et al. Mapping of transcription factor motifs in active chromatin identifies IRF5 as key regulator in classical Hodgkin lymphoma. Proc Natl Acad Sci U S A 111, E4513–4522 (2014). [PubMed: 25288773]
39. Dominguez CX et al. The transcription factors ZEB2 and T-bet cooperate to program cytotoxic T cell terminal differentiation in response to LCMV viral infection. J Exp Med 212, 2041–2056 (2015). [PubMed: 26503446]
40. Barwick BG , Scharer CD , Bally APR & Boss JM Plasma cell differentiation is coupled to division-dependent DNA hypomethylation and gene regulation. Nat Immunol 17, 1216–1225 (2016). [PubMed: 27500631]
41. Karwacz K et al. Critical role of IRF1 and BATF in forming chromatin landscape during type 1 regulatory cell differentiation. Nat Immunol 18, 412–421 (2017). [PubMed: 28166218]
42. Audzevich T , Pearce G , Breucha M , Gunal G & Jessberger R Control of the STAT6-BCL6 antagonism by SWAP-70 determines IgE production. J Immunol 190, 4946–4955 (2013). [PubMed: 23589612]
43. Ochiai K et al. Transcriptional regulation of germinal center B and plasma cell fates by dynamical control of IRF4. Immunity 38, 918–929 (2013). [PubMed: 23684984]
44. Kang K et al. Interferon-gamma Represses M2 Gene Expression in Human Macrophages by Disassembling Enhancers Bound by the Transcription Factor MAF. Immunity 47, 235–250 e234 (2017). [PubMed: 28813657]
45. Carotta S et al. The transcription factors IRF8 and PU.1 negatively regulate plasma cell differentiation. J Exp Med 211, 2169–2181 (2014). [PubMed: 25288399]
46. Lu D et al. The miR-155-PU.1 axis acts on Pax5 to enable efficient terminal B cell differentiation. J Exp Med 211, 2183–2198 (2014). [PubMed: 25288398]
47. Sarra M , Pallone F & Monteleone G Interleukin-21 in chronic inflammatory diseases. Biofactors 39, 368–373 (2013). [PubMed: 23553807]

48. Eames HL , Corbin AL & Udalova IA Interferon regulatory factor 5 in human autoimmunity and murine models of autoimmune disease. Transl Res 167, 167–182 (2016). [PubMed: 26207886]

49. Claes N et al. Age-Associated B Cells with Proinflammatory Characteristics Are Expanded in a Proportion of Multiple Sclerosis Patients. J Immunol 197, 4576–4583 (2016). [PubMed: 27837111]

50. Wang Z et al. T-bet-Expressing B Cells Are Positively Associated with Crohn's Disease Activity and Support Th1 Inflammation. DNA Cell Biol 35, 628–635 (2016). [PubMed: 27348235]

51. Biswas PS et al. Phosphorylation of IRF4 by ROCK2 regulates IL-17 and IL-21 production and the development of autoimmunity in mice. J Clin Invest 120, 3280–3295 (2010). [PubMed: 20697158]

52. Biswas PS , Kang K , Gupta S , Bhagat G & Pernis AB A murine autoimmune model of rheumatoid arthritis and systemic lupus erythematosus associated with deregulated production of IL-17 and IL-21. Methods Mol Biol 900, 233–251 (2012). [PubMed: 22933072]

53. Minnich M et al. Multifunctional role of the transcription factor Blimp-1 in coordinating plasma cell differentiation. Nat Immunol 17, 331–343 (2016). [PubMed: 26779602]

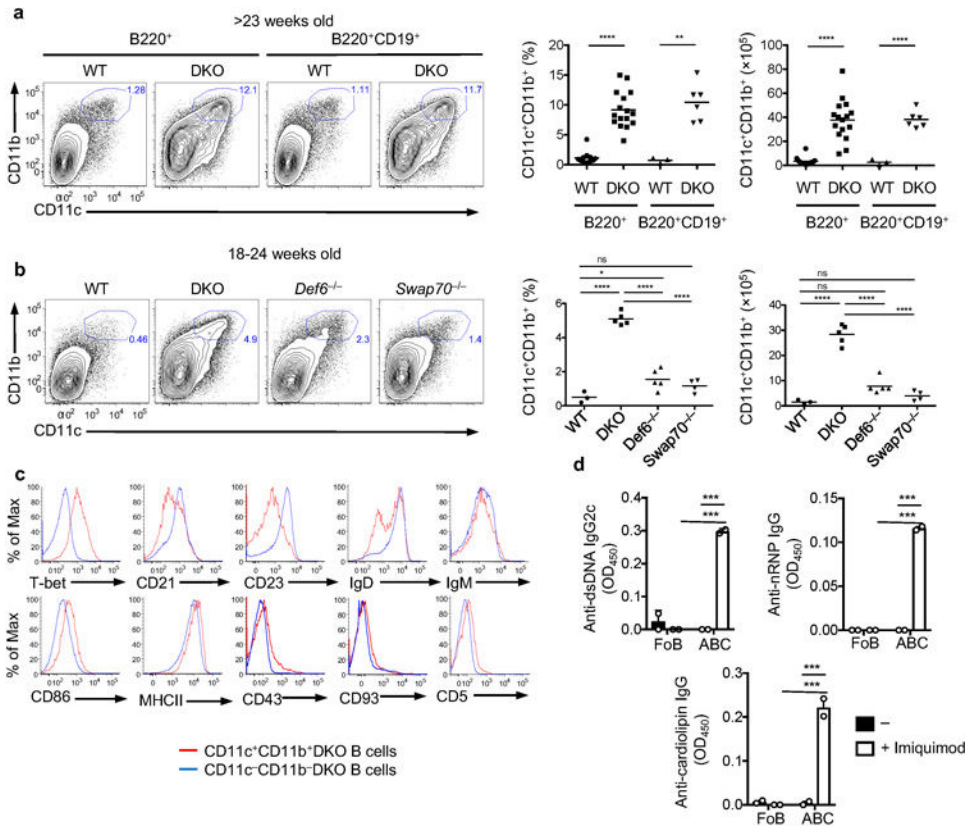

Figure 1. Spontaneous expansion of ABCs in DKO mice.

(**a**) Flow cytometry of B220$^+$ or B220$^+$CD19$^+$ cells from the spleens of WT and DKO female mice (>23 weeks-old) analyzing CD11c and CD11b expression. Graphs show frequencies and numbers for individual mice and mean values of 3 independent experiments for B220$^+$CD19$^+$ (n = 3 WT and 6 DKO) and 8 independent experiments for B220$^+$ (n = 12 WT and 16 DKO). ** $P = 0.0014$; **** $P < 0.0001$. (two-tailed Student's *t*-test). (**b**) Flow cytometry of B220$^+$CD19$^+$ cells from the spleens of WT, DKO, *Def6*$^{-/-}$ and *Swap70*$^{-/-}$ female mice (18–24 weeks old) analyzing CD11c and CD11b. Graphs show frequencies and numbers for individual mice and mean values of 3 independent experiments (n = 3 WT, 4 *Swap70*$^{-/-}$, and 5 *Def6*$^{-/-}$ and DKO). * $P = 0.0403$; **** $P < 0.0001$ (One-way ANOVA, followed by Bonferroni's multiple comparisons test). (**c**) Histograms showing the expression of the indicated markers on B220$^+$CD19$^+$CD11c$^+$CD11b$^+$ and B220$^+$CD19$^+$CD11c$^-$CD11b$^-$ cells in the spleens of DKO female mice (>18 weeks old). Data are representative of 7 independent experiments, n = 11 mice (T-bet, CD21, CD23); 4 independent experiments, n = 6 mice (CD86 and MHCII); 3 independent experiments, n = 5 mice (IgD, IgM, CD43, CD93) and 2 independent experiments, n = 4 mice (CD5). (**d**) Abundance of anti-dsDNA IgG2c, anti-nRNP, and anti-cardiolipin IgG antibodies in the supernatants of sorted ABC (B220$^+$CD19$^+$CD11c$^+$CD11b$^+$) and FoB (B220$^+$CD19$^+$CD11c$^-$CD11b$^-$CD23$^+$) B cells stimulated *in vitro* ± 1 μg/ml imiquimod for 7 days as measured by ELISA. One representative experiment of 4 independent experiments is shown (n= 4 cell cultures). Mean ± SEM of technical replicates (circles) is shown. *** $P = 0.0004$ (anti-dsDNA IgG2c); *** P

< 0.0001 (anti-nRNP IgG) and *** $P = 0.0007$ (One-way ANOVA, followed by Bonferroni's multiple comparisons test).

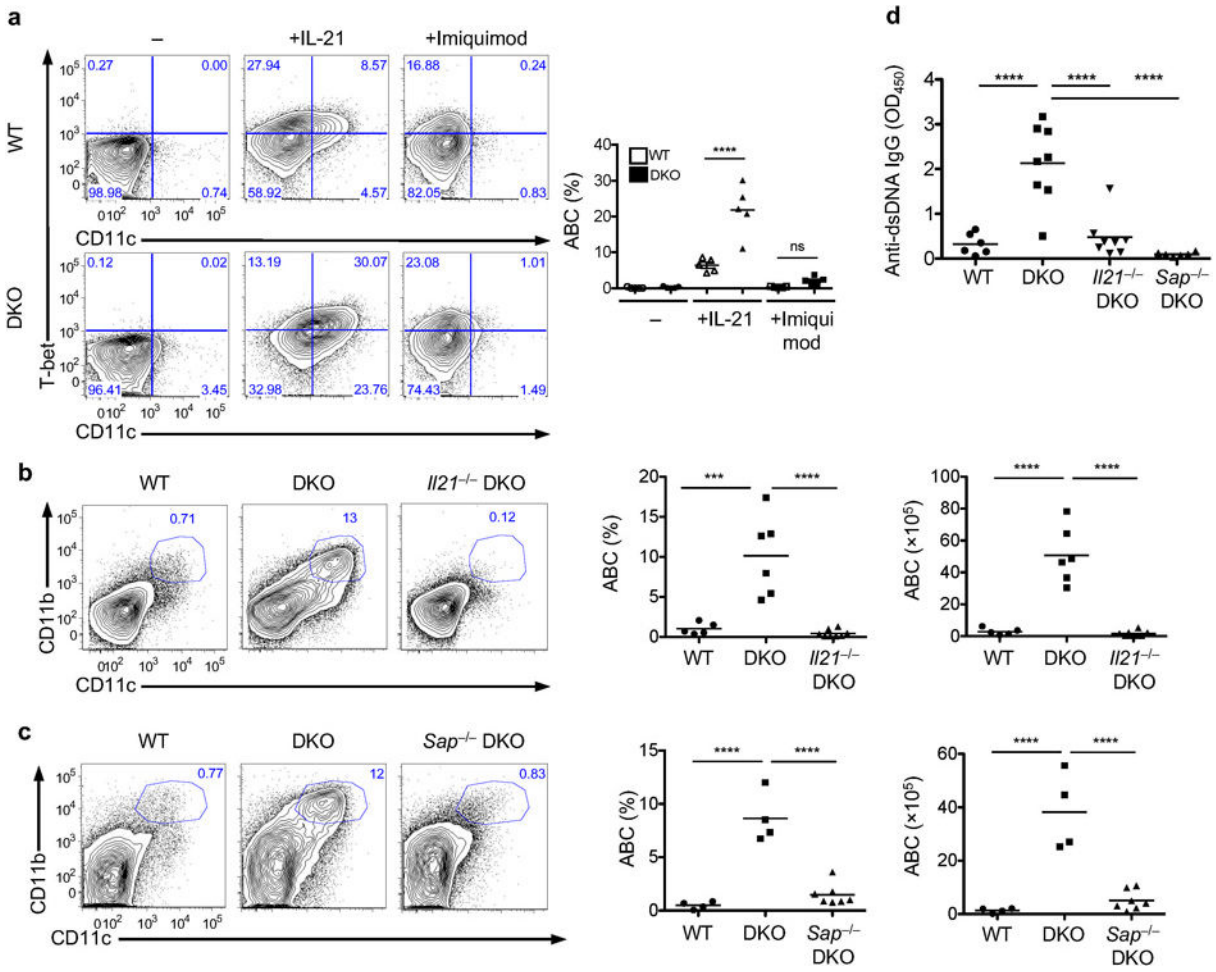

Figure 2. IL-21 regulates the generation of DKO ABCs *in vitro* and *in vivo*.

(**a**) Generation of ABCs ($B220^+CD11c^+T\text{-}bet^+$) from cultures of $CD23^+$ B cells purified from WT and DKO female mice (8–10 weeks of age) stimulated with αIgM (5 μg/ml), αCD40 (5 μg/ml), IL-21 (50 ng/ml) or imiquimod (1 μg/ml) for 3 days as assessed by flow cytometry. Graph shows mean and individual values of 5 independent experiments (n = 5 cell cultures). **** $P < 0.0001$. (One-way ANOVA followed by Bonferroni's multiple comparisons test). (**b**) Flow cytometry of $B220^+$ cells from the spleens of WT, DKO, and *Il21*$^{-/-}$ DKO female mice (>24 weeks old) analyzing CD11c and CD11b expression. Graphs show frequencies and numbers of ABCs ($B220^+CD11c^+CD11b^+$) in individual mice and mean value of 4 independent experiments (n = 5 WT, 6 DKO and 8 *Il21*$^{-/-}$ DKO mice). *** $P = 0.0002$; **** $P < 0.0001$. (One-way ANOVA followed by Bonferroni's multiple comparisons test). (**c**) Flow cytometry of $B220^+$ cells from the spleens of WT, DKO, and *Sap*$^{-/-}$ DKO female mice (>24 weeks old) analyzing CD11c and CD11b expression. Graphs show frequencies and numbers of ABCs ($B220^+CD11c^+CD11b^+$) in individual mice and mean value of 4 independent experiments (n = 4 WT, 4 DKO, and 7 *Sap*$^{-/-}$ DKO mice). **** $P < 0.0001$. (One-way ANOVA followed by Bonferroni's multiple comparisons test). (**d**) Anti-dsDNA antibodies in the sera of WT, DKO, *Il21*$^{-/-}$ DKO, and *Sap*$^{-/-}$ DKO mice were analyzed by ELISA. Graphs show data of individual mice and mean value of 4

independent experiments (n = 6 WT, 8 DKO, 8 *Il21*$^{-/-}$ DKO, and 6 *Sap*$^{-/-}$ DKO). **** $P <$ 0.0001. (One-way ANOVA followed by Bonferroni's multiple comparisons test).

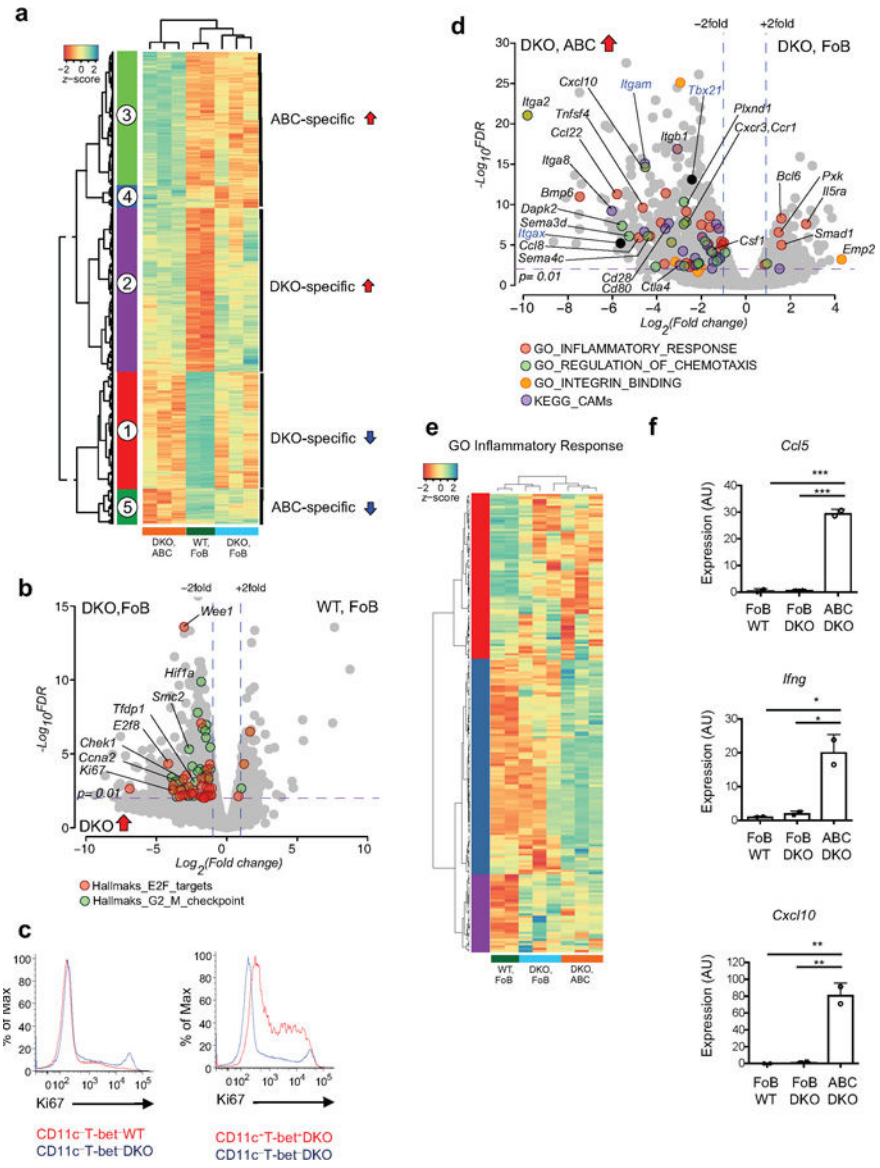

Figure 3. DKO ABCs exhibit a distinctive transcriptome.

(**a**) Hierarchical clustering of log-transformed counts per million (cpm) for differentially expressed genes identified by RNAseq analysis of RNA from FACS sorted FoB ($B220^+CD19^+CD11c^-CD11b^-CD23^+$) cells from WT and DKO female mice and ABC ($B220^+CD19^+CD11c^+CD11b^+$) cells from DKO female mice (>20 weeks old). (n=2 WT, 3 DKO). (**b**) Volcano plot comparing gene expression in WT and DKO FoB. Colors indicate differentially expressed genes (FDR corrected P <0.01, Fold change >2; WT FoB/DKO FoB, n= 2 WT, 3 DKO) belonging to selected GSEA Hallmark pathways as indicated. (**c**) Proliferation of $B220^+CD11c^-$T-bet$^-$cells in the spleens of WT and DKO female mice (>23 weeks old, left panel) or of $B220^+CD11c^-$T-bet$^-$cells and $B220^+CD11c^+$T-bet$^+$ (ABCs) in the spleens of DKO female mice (>23 weeks old, right panel) as assessed by Ki67 staining and flow cytometry. Representative histogram of 4 and 5 independent experiments, respectively is shown (n= 5 and 6 mice/group, respectively). (**d**) Volcano plot comparing

gene expression in FoB ($B220^+CD19^+CD11c^-CD11b^-CD23^+$) and ABC ($B220^+CD19^+CD11c^+CD11b^+$) cells sorted from DKO female mice (>20 weeks old). Colors indicate differentially expressed genes (FDR corrected $P < 0.01$, Fold change >2, DKOFoB/DKO ABC, n= 3 mice) belonging to selected GSEA pathways as indicated. (**e**) Hierarchical clustering of log-transform counts per million (cpm) for genes that belong to the GO_inflammatory_response gene set (MsigDB) identified by RNA-Seq analysis of RNA from FACS sorted FoB ($B220^+CD19^+CD11c^-CD11b^-CD23^+$) and ABC ($B220^+CD19^+CD11c^+CD11b^+$) cells from WT and DKO female mice (n=2 WT, 3 DKO), Pearson's correlation was used as distance metric between genes. (**f**) qPCR analysis of the expression of *Ccl5, Ifng, and Cxcl10* mRNA in sorted FoB ($B220^+CD19^+CD11c^-CD11b^-CD23^+$) cells from WT and DKO female mice and ABC ($B220^+CD19^+CD11c^+CD11b^+$) cells from DKO female mice as indicated. The data were normalized relative to *Ppia* mRNA expression. Mean of one representative experiment of 2 (*Ccl5*) or 3 (*Ifng* and *Cxcl10*) independent experiments is shown. n = 2 mice (*Ccl5*) and 3 mice (*Ifng* and *Cxcl10*). SEM of technical replicates (circles) is shown. * $P = 0.0242$ (FoB WT vs. ABC DKO *Ifng)* and $P = 0.0282$ (FoB DKO vs. ABC DKO *Ifng*); ** $P = 0.0068$ (FoB WT vs. ABC DKO) and $P = 0.0072$ (FoB DKO vs. ABC DKO); *** $P = 0.0002$ (*Ccl5*). (one-way ANOVA followed by Bonferroni's multiple comparisons test).

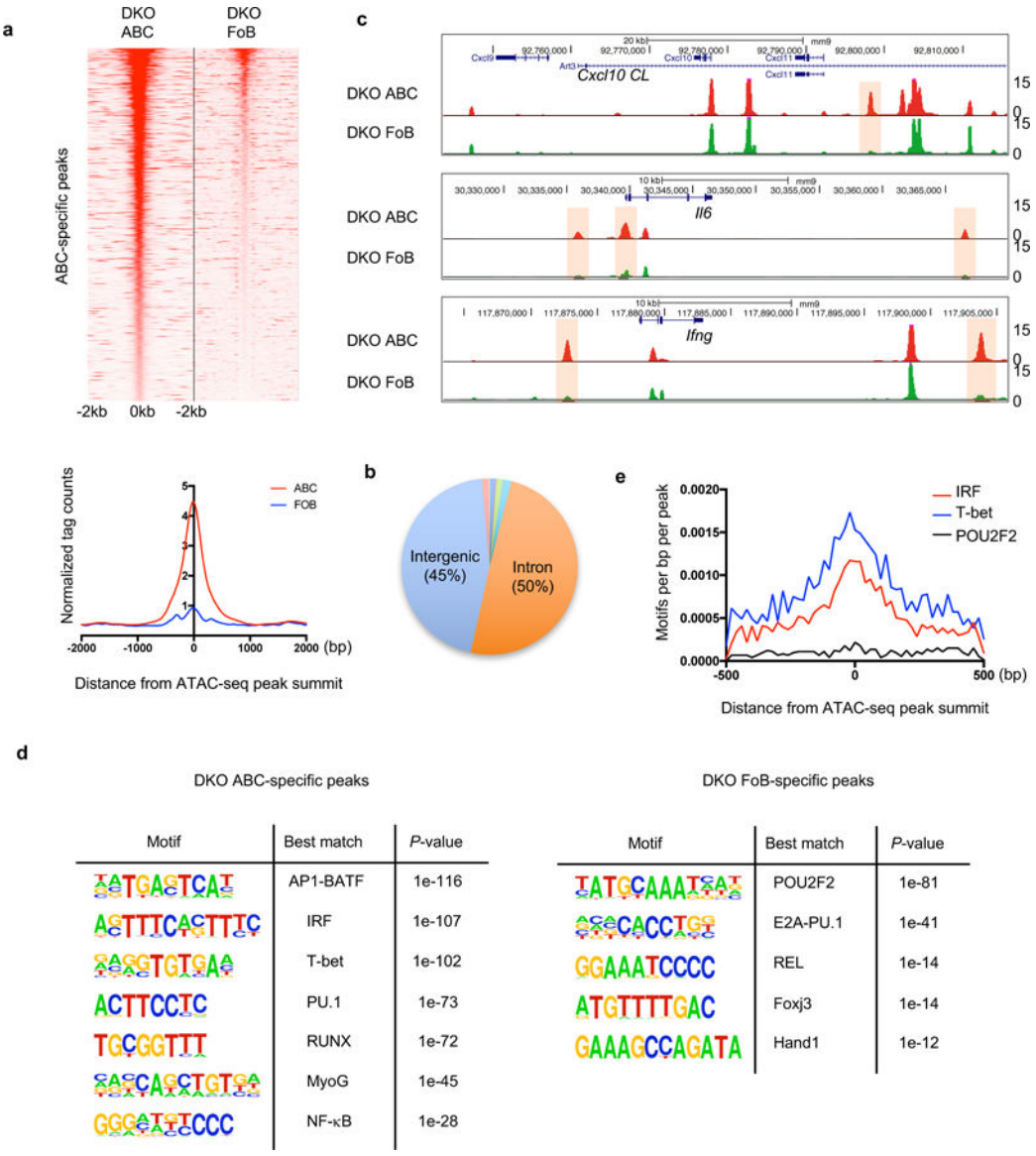

Figure 4. The chromatin landscape of DKO ABCs is enriched in IRF and AP-1-BATF motifs.

(**a**) Normalized ATAC-seq tag density distributions for 4kb window centered at the summit of ABC-specific peaks (n=3,666, top panel) and average distribution of ATAC-seq normalized tag densities (bottom). (n=2/group). (**b**) Genomic distribution of ABC-specific peaks of ATAC-seq relative to annotated genomic features. (**c**) Normalized ATAC-seq tag distributions tracks for representative genomic regions at *Cxcl10 cluster*, *Il6*, and *Ifng* genes. Highlighted are ABC-specific ATAC-seq peaks. (**d**) *De novo* motif enrichment analysis in ABC-specific and FoB-specific ATAC-seq peaks. The binomial distribution is used to score motifs (a 95% confidence level) (**e**) Motif density distribution relative to the peak summit for IRF, T-bet and POU2F2 motifs in ABC-specific ATAC-seq peaks. Data are from one representative out of two independent experiments with similar results (c-e).

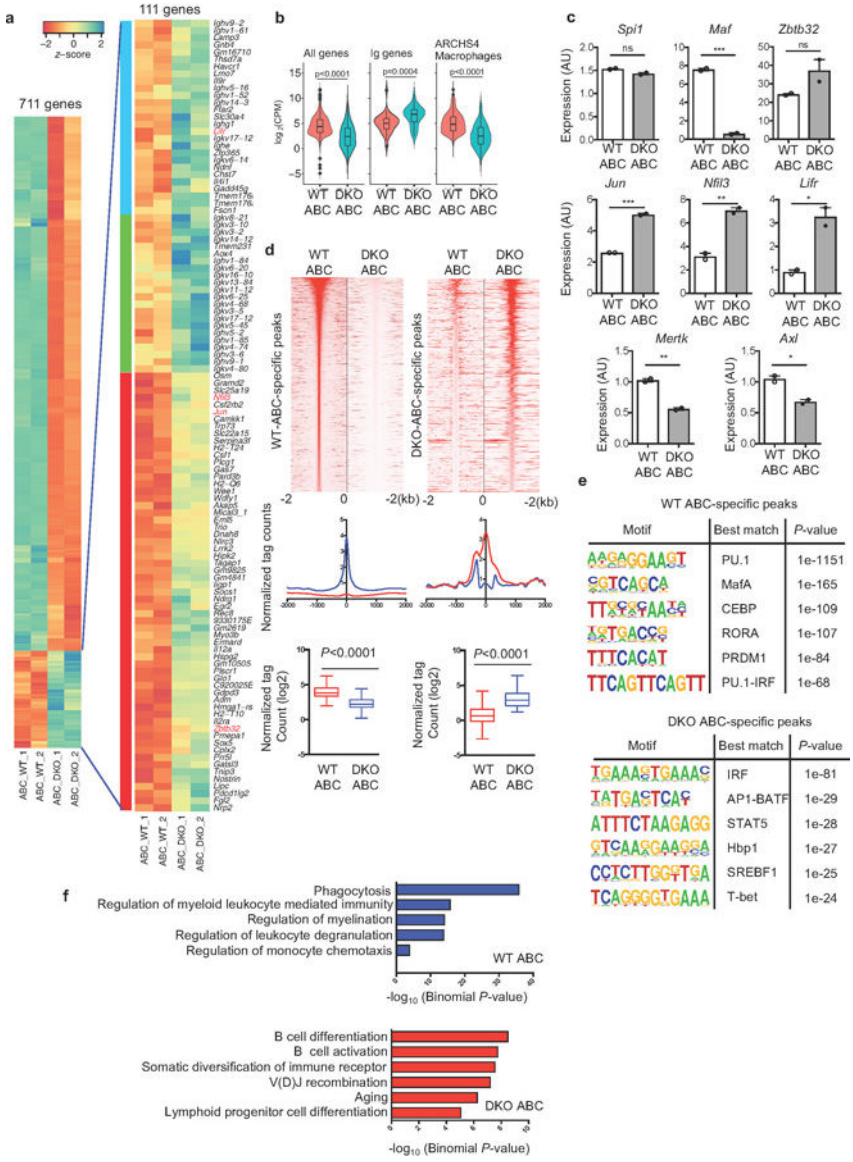

Figure 5. WT and DKO ABCs exhibit distinct transcriptional and chromatin profiles.

(**a**) Hierarchical clustering of log-transformed counts per million (cpm) for differentially expressed genes identified by RNAseq analysis of RNA from FACS sorted ABC ($B220^+CD19^+CD11c^+CD11b^+$) cells from WT and DKO female mice (>33 weeks old). (n= 2 mice/group). (**b**) Violin plot combines basic gene expression summary statistics for each indicated set of genes including the median expression (horizontal line), first and third quartiles (vertical box bounds), the value spread (central vertical line bound at 1.5 interquartile range) and the outliers (black circles) with the kernel density estimate of expression values distribution. Pairwise comparisons of gene set expression values in WT and DKO ABC cells for all differentially expressed genes (n=713, $p<2.2*10^{-16}$, Z=16.65, CI 95%[1.952 , 2.415]), Ig genes (n=34,p=0.00044, Z= −3.44 , 95% CI[−2.4170, −0.8235]) and ARCHS4 Macrophages signature (n=252, $p<2.2*10^{-16}$, Z= 11.521, 95% CI[2.148 2.9175] http://amp.pharm.mssm.edu/archs4/index.html) was performed using approximative

Wilcoxon-Mann-Whitney test. (**c**) qPCR analysis of the expression of representative genes in sorted ABC ($B220^+CD19^+CD11c^+CD11b^+$) cells from WT and DKO female mice as indicated. The data were normalized relative to *Ppia* mRNA expression. Mean of one representative experiment of 2 independent experiments is shown (n = 2 mice/group). SEM of technical replicates (circles) is shown. ns: not significant; * $P = 0.0273$ (*Lifr*) and $P = 0.0254$ (*Axl*); ** $P = 0.0081$ (*Nfil3*) and $P = 0.0054$ (*Mertk*); *** $P = 0.0007$ (*Maf*) and $P = 0.0003$(*Jun*) (two-tailed Student's t-test). (**d**) Normalized ATAC-seq tag density distributions for 4kb window centered at the summit of WT-specific (left, n=27,483) or DKO-specific (right, n=1583) peaks and average distribution of ATAC-seq normalized tag densities (bottom). (Kolmogorov-Smirnov test). (**e**) *De novo* motif enrichment analysis in WT-specific and DKO-specific ATAC-seq peaks. The binomial distribution is used to score motifs (a 95% confidence level). (**f**) Functionally enriched Gene Ontology (GO) categories of WT-specific and DKO-specific peaks of ATAC-seq. Data are from one representative out of two independent experiments with similar results (d-f).

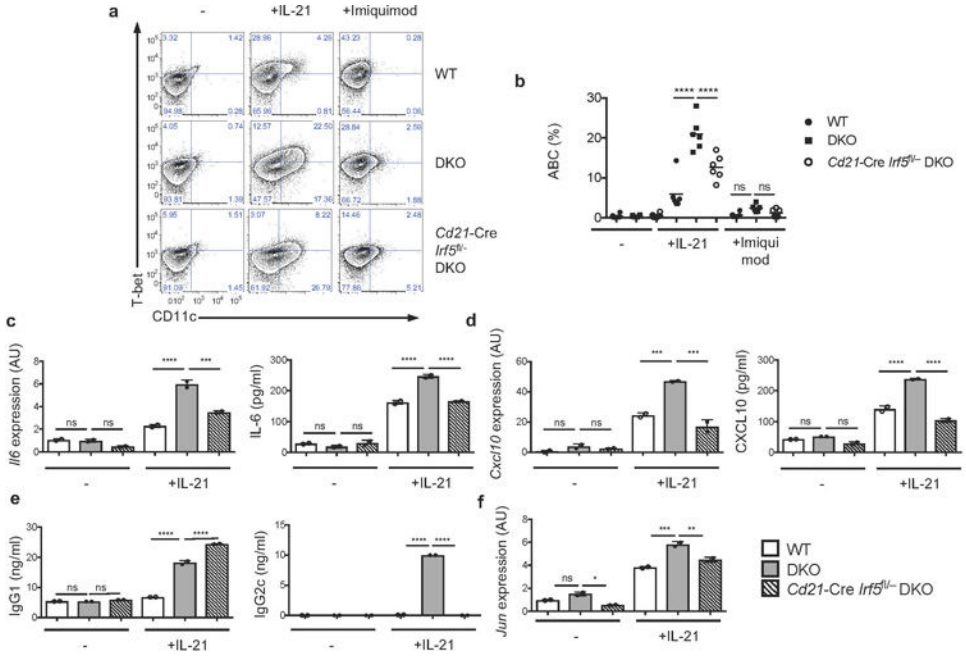

Figure 6. IRF5 regulates the IL-21-mediated formation of DKO ABCs.

(**a**) Generation of ABCs ($B220^{+}CD11c^{+}T\text{-}bet^{+}$) from cultures of $CD23^{+}$ B cells purified from WT, DKO, and *Cd21*-Cre $Irf5^{fl/-}$DKO female mice (8–10 weeks of age) stimulated with αIgM (5 μg/ml), αCD40 (5 μg/ml), IL-21 (50 ng/ml) or imiquimod (1 μg/ml) for 3 days as assessed by flow cytometry. Representative data of 6 independent experiments (n = 6 cell cultures) is shown. (**b**) Quantification of **a**. Graph shows mean and individual values of 6 independent experiments. ** $P = 0.0052$ (DKO+IL-21 vs. *Cd21*-Cre $Irf5^{fl/-}$DKO +IL-21) and $P = 0.0095$ (WT+Imiquimod vs. DKO+Imiquimod); **** $P < 0.0001$. (One-way ANOVA followed by Bonferroni's multiple comparisons test). (**c,d**) Analysis of the expression and production of IL-6 and CXCL10 in cultures of cells stimulated ± IL-21 as in **a** as assessed by qPCR and ELISA. qPCR data were normalized relative to *Ppia* mRNA expression. One representative experiment of 3 independent experiments is shown (n= 3 cell cultures). Mean ± SEM of technical replicates (circles) is shown. ns: not significant; *** $P = 0.0009$ (*Il6*), $P = 0.0007$ (*Cxcl10* WT+IL-21 vs. DKO+IL-21) and $P = 0.001$ (*Cxcl10* DKO +IL-21 vs. *Cd21*-Cre $Irf5^{fl/-}$DKO+IL-21); **** $P < 0.0001$. (One-way ANOVA followed by Bonferroni's multiple comparisons test) (**e**) Supernatants of cells stimulated ± IL-21 as in **a** for 7 days were analyzed by ELISA. Data are representative of 3 independent experiments (n= 3 cell cultures). Mean ± SEM of technical replicates (circles) is shown. ns: not significant; **** $P < 0.0001$ (One-way ANOVA followed by Bonferroni's multiple comparisons test). (**f**) qPCR analysis of the expression of *Jun* in cultures of cells stimulated ± IL-21 as in **a.** Data were normalized relative to *Ppia* mRNA expression. One representative experiment of 2 independent experiments is shown (n= 2 cell cultures). Mean ± SEM of technical replicates (circles) is shown. * $P = 0.0104$; ** $P = 0.0018$; *** $P = 0.0002$ (One-way ANOVA followed by Bonferroni's multiple comparisons test).

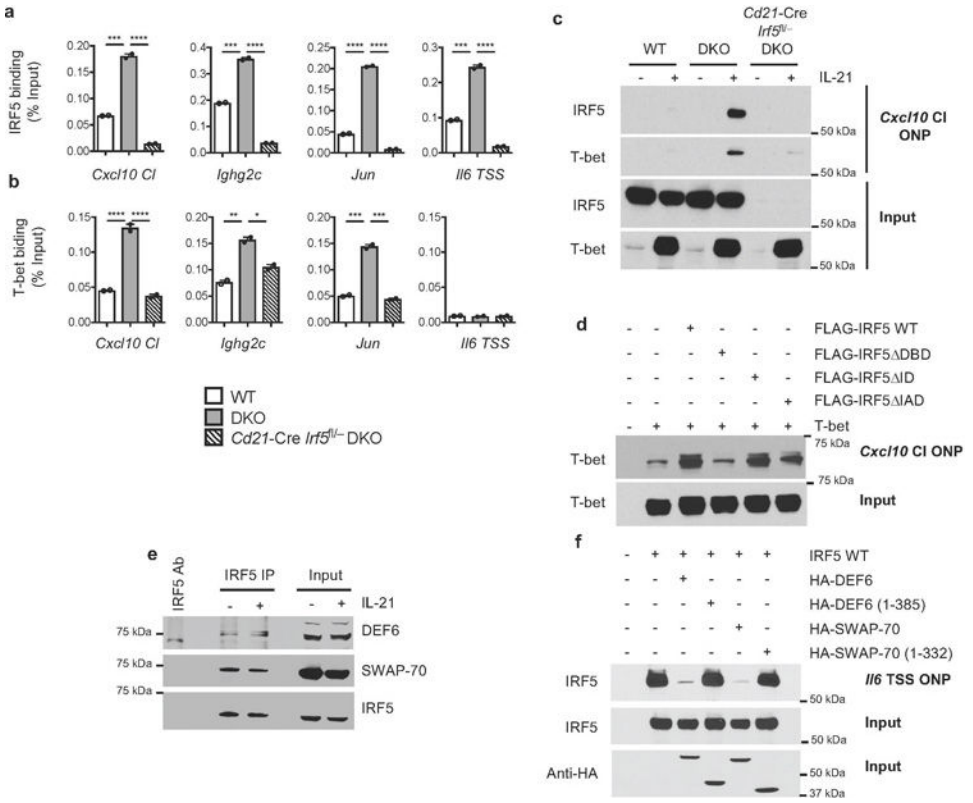

Figure 7. Enhanced binding of IRF5 to ABCs regulatory regions in the absence of the SWEF proteins.

(**a**) ChIP assays were performed with an IRF5 antibody on CD23^{+} B cells purified from WT, DKO, and *Cd21*-Cre *Irf5*$^{fl/–}$DKO female mice (8–10 weeks of age) stimulated with αIgM (5 μg/ml), αCD40 (5 μg/ml), and IL-21 (50 ng/ml) for 2 days. Immunoprecipitated DNA was analyzed by qPCR using primers within the ABC-specific ATAC-seq peaks at the *Cxcl10* cluster (Cl), *Ighg2c*, *Jun*, and the *Il6* TSS. One representative experiment of 4 (*Il6* TSS and *Cxcl10* Cl, n= 4 cell cultures) or 2 (*Ighg2c* and *Jun*, n= 2 cell cultures) independent experiments is shown. Mean ± SEM of technical replicates (circles) is shown. *** P = 0.0002 (*Cxcl10*) and P = 0.0001 (*Ighg2c* and *Il6* TSS); **** P < 0.0001 (One-way ANOVA followed by Bonferroni's multiple comparisons test). (**b**) ChIP assay were performed with a T-bet antibody as in **a**. One representative experiment of 4 (*Il6* TSS and *Cxcl10* Cl, n= 4 cell cultures) or 2 (*Ighg2c* and *Jun,* n= 2 cell cultures) independent experiments is shown. Mean ± SEM of technical replicates (circles) is shown. * P = 0.0119; ** P = 0.0033; *** P = 0.0004 (WT vs. DKO) and P = 0.0003 (DKO vs. *Cd21*-Cre *Irf5*$^{fl/–}$DKO); **** P < 0.0001 (One-way ANOVA followed by Bonferroni's multiple comparisons test). (**c**) Nuclear extracts were prepared from cells stimulated with αIgM (5 μg/ml), αCD40 (5 μg/ml) +/− IL-21 (50 ng/ml) as in **a** and subjected to ONP assay with a biotinylated oligonucleotide from the *Cxcl10* Cl. Precipitated proteins were analyzed by immunoblotting with an IRF5 and T-bet antibody as indicated. Data are representative of 2 independent experiments. (**d**) 293T cells were transiently transfected as indicated. Nuclear extracts were prepared and subjected to ONP assay with a biotinylated oligonucleotide from the *Cxcl10* Cl. Precipitated proteins were analyzed by immunoblotting with a T-bet antibody. Data are representative of

2 independent experiments. (**e)** IRF5/SWEF proteins co-immunoprecipitation from nuclear extracts of cells stimulated with or without IL-21 as in **a** for 2 days. Immunoprecipitation was performed with an IRF5 antibody and probed with a DEF6, SWAP-70, or IRF5 antibody as indicated. Data are representative of 2 independent experiments. (**f**) 293T cells were transiently transfected as indicated. Nuclear extracts were prepared and subjected to ONP assay with a biotinylated oligonucleotide from the IL-6 TSS. Precipitated proteins were analyzed by immunoblotting with an IRF5 antibody. Data are representative of 2 independent experiments.

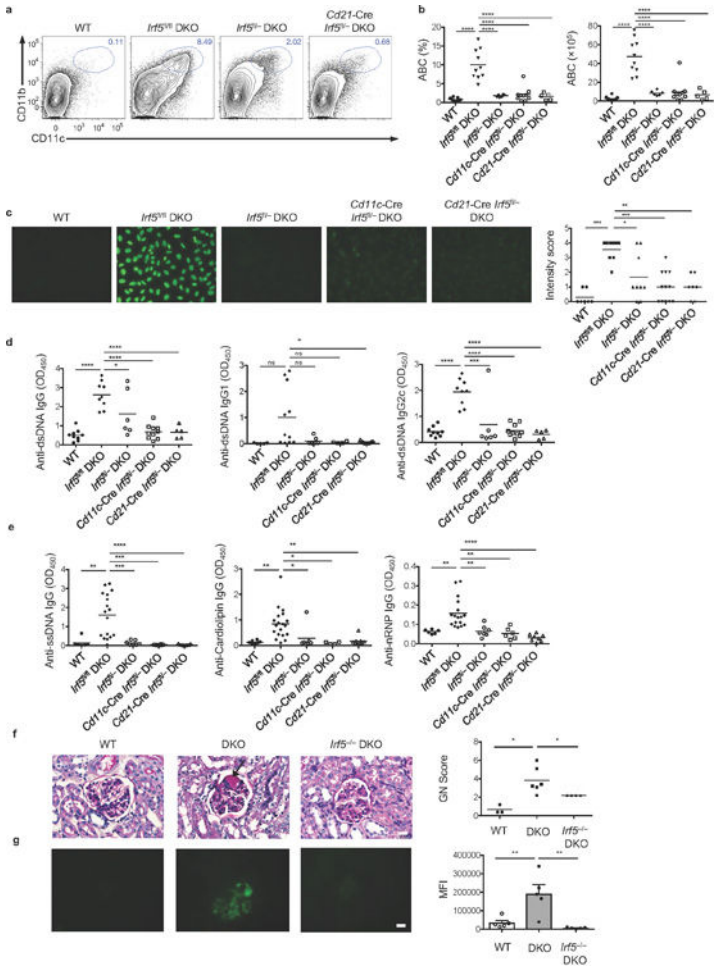

Figure 8. Monoallelic deletion of *Irf5* abolishes accumulation of ABCs and lupus development in DKO mice.

(**a**) Flow cytometric analysis of $CD11c^{+}CD11b^{+}$ B cells in the spleens of WT, $Irf5^{fl/fl}$ DKO, $Irf5^{fl/-}$ DKO and *Cd21*-Cre $Irf5^{fl/-}$ DKO female mice (>20 weeks-old). Representative FACS plots for CD11c and CD11b expression is shown. (**b**) Quantification of **a**. Graphs show frequencies and numbers for individual mice and mean value of 10 independent experiments (n= 9 WT, 10 $Irf5^{fl/fl}$ DKO, 10 $Irf5^{fl/-}$ DKO, 10 *Cd11c*-Cre $Irf5^{fl/-}$ DKO and 5 *Cd21*-Cre $Irf5^{fl/-}$ DKO mice). **** P < 0.0001. (One-way ANOVA followed by Bonferroni's multiple comparisons test). (**c**) Antinuclear Antibodies (ANAs) were determined in sera (1:200) of the indicated mice (>20 weeks old). Fluorescence intensity was scored as described in Materials and Methods. Graph shows score of individual mice and mean value of 10 independent experiments (n= 7 WT, 9 $Irf5^{fl/fl}$ DKO, 9 $Irf5^{fl/-}$ DKO, 12 *Cd11c*-Cre $Irf5^{fl/-}$ DKO and 7 *Cd21*-Cre $Irf5^{fl/-}$ DKO mice). * $P = 0.0142$; ** $P = 0.004$ and *** P < 0.0001 (Mann-Whitney test). (**d**) Anti-dsDNA IgG, IgG1, or IgG2c antibodies in the indicated mice (>20 weeks old) were analyzed by ELISA. Graphs show values for individual mice and mean value of 10 independent experiments. n= 9 (IgG, IgG2c) and 5 (IgG1) WT, 9 (IgG, IgG2c) and 11 (IgG1) $Irf5^{fl/fl}$ DKO, 6 $Irf5^{fl/-}$ DKO, 10 (IgG, IgG2c) and 4 (IgG1) *Cd11c*-Cre $Irf5^{fl/-}$ DKO and 5 (IgG, IgG2c) and 9 *Cd21*-Cre $Irf5^{fl/-}$ DKO mice. * $P = 0.0206$(IgG) and $P = 0.0280$ (IgG1); *** $P = 0.003$; **** $P < 0.0001$. (One-way ANOVA followed by

Bonferroni's multiple comparisons test). (**e**) Anti-ssDNA, anti-cardiolipin, and anti-nRNP IgG antibodies in the sera of the indicated mice (>20 weeks old) were analyzed by ELISA. Graphs show values for individual mice and mean value of 10 independent experiments. n= 6 (ssDNA, nRNP) and 8 (Cardiolipin) WT, 17 (ssDNA, nRNP) and 19 (Cardiolipin) *Irf5*$^{fl/fl}$ DKO, 7 *Irf5*$^{fl/-}$ DKO, 6 (ssDNA, nRNP) and 4 (Cardiolipin) *Cd11c*-Cre *Irf5*$^{fl/-}$ DKO, and 9 (ssDNA, Cardiolipin) and 8 (nRNP) *Cd21*-Cre *Irf5*$^{fl/-}$ DKO mice. * $P < 0.05$; ** $P < 0.01$; *** $P < 0.001$; **** $P < 0.0001$. (One-way ANOVA followed by Bonferroni's multiple comparisons test). (**f**) Representative PAS staining and glomerulonephritis score of WT, DKO, and *Irf5*$^{-/-}$ DKO mice (which include *Cd11c*-Cre *Irf5*$^{fl/-}$ DKO and *Cd21*-Cre *Irf5*$^{fl/-}$ DKO mice). Score of individual mice and mean value of 3 independent experiments are shown. n= 3 WT, 6 DKO, and 4 *Irf5*$^{-/-}$ DKO mice. * $P = 0.0275$ (WT vs. DKO) and $P = 0.0307$ (DKO vs. *Irf5*$^{-/-}$ DKO) (Mann-Whitney test). Scale bar= 20 μm (**g**) Representative IgG deposition in the kidney of WT, DKO, and *Irf5*$^{-/-}$ DKO mice (which include *Cd11c*-Cre *Irf5*$^{fl/-}$ DKO and *Cd21*-Cre *Irf5*$^{fl/-}$ DKO mice). MFI quantification show individual (circles) and mean values of 5 renal sections in one mouse representative of 3 independent experiments. n= 3 WT, 6 DKO and 4 *Irf5*$^{-/-}$ DKO mice. * $P = 0.0071$ (WT vs. DKO) and $P = 0.0021$ (DKO vs. *Irf5*$^{-/-}$ DKO**)**. Scale bar= 30 μm.